Euro. Jnl of Applied Mathematics (2004), *vol.* 15, *pp.* 409–450.
DOI: 10.1017/S0956792504005546 Printed in the United Kingdom

Flow performance of horizontal wells with inflow control devices

C. ATKINSON[1], F. MONMONT[2] and A. F. ZAZOVSKY[3]

[1] *Department of Mathematics, Imperial College, London SW7 2BZ, UK*
[2] *Schlumberger Cambridge Research, High Cross, Madingley Road Cambridge CB3 0EL, UK*
[3] *Schlumberger Oilfield Services, Sugar Land Product Center, MD 110-6, 110 Schlumberger Drive, Sugar Land, TX 77478, USA*

(*Received 22 July 2002; revised 7 May 2003*)

This paper presents a powerful approximate method for modelling the steady single-phase flow into a horizontal well completed with an Inflow Control Device (ICD) in an anisotropic reservoir. Two types of problems are investigated: the forward problem, which allows the user to find the flux distribution along the wellbore for a specified pressure drawdown, and the inverse problem to determine the ICD properties when the flux or reservoir pressure drawdown along the wellbore is given. The method is based on structuring the flow patterns around and, inside the wellbore and across the ICD and on the reduction of the dimensionality of the problem by using boundary integral equations. The resulting one dimensional singular nonlinear integro-differential equation is solved numerically, using the appropriate quadrature formula for singular integrals with Cauchy kernels.

1 Introduction

This study was motivated by the problem of Inflow Control Devices (ICD) for horizontal wells with sand control completions (a completion is a string of tubes lining the wellbore). The completion is perforated to enable the inflow of hydrocarbons from the formation into the wellbore, but should prevent sand invasion from the formation. The main focus in this study is on the refinement of a hydrodynamic model, to provide better coupling of the reservoir flow with the flow across the ICD and inside its basepipe. This enhancement is necessary for a better estimation of the flow performance of horizontal wells completed with ICD (the forward problem) and also for the determination of ICD properties (the inverse problem) in order to achieve, say, uniform drainage of a reservoir. The second usage is important because an ICD is designed as a passive inflow control device and therefore its tuning prior to installation will be critical for the completion performance during the entire production life of a horizontal wellbore.

The problem of reservoir development by long horizontal wells with sand control completions must account for the frictional pressure losses due to blockage caused by installed screens or liners. It is known that the frictional pressure drop along a pipe with impermeable walls, Δp_f, is proportional to L/d_s^{α}, where L is the length of the pipe, d_s is its diameter and the exponent α varies from 3 for a laminar flow to approximately 4.5 for a turbulent flow. For this reason, even a small restriction of the wellbore cross-sectional area may induce a significant increase in the pressure loss along its length. Moreover, the

diameters of basepipes of sand control devices can be much smaller than their external diameters. This creates pressure losses along the horizontal wellbore comparable to the applied drawdown pressure and therefore restricts the effective length of the horizontal wellbore. At the same time, the pressure variation along the wellbore results in a non-uniform reservoir drainage and leads to the premature water breakthrough into the wellbore near its heel, the coning effect [4].

The aim of an ICD is to compensate for the expected pressure variation along the wellbore by profiling the pressure drop across it. This should allow one to achieve uniform drainage of a reservoir. This problem is challenging because it requires the coupling of the flows in the reservoir, across the ICD and inside the basepipe. The main difficulties are that the reservoir flow is three-dimensional and is on multiple scales, which vary from a few millimetres (the diameter of holes in the ICD basepipe), a few centimetres (the wellbore radius) to a few hundred metres (the wellbore length and the distance between wells). The problem is also nonlinear because of the turbulent flows in the ICD basepipe and through the holes in it. All this has forced previous investigators to use either approximate solutions, based on additional assumptions, or numerical simulators, which usually have limited resolution and accuracy or are very time-consuming [3, 5–9, 12, 15, 16].

The approach developed in this report is based upon the idea of flow structuring, which allows one to reduce the dimensionality of the complex multi-scale problem, using the fact that the three-dimensional effects are localised in the vicinities of the toe and heel of the horizontal wellbore only. Indeed, the flow inside the reservoir is a one-dimensional plane flow far from the wellbore and is locally two-dimensional near the wellbore except near the vicinities of its toe and heel, which are small compared to the wellbore length. The general solution of Laplace's equation for a half plane in the form of the Poisson integral can be used to describe the far field flow around the horizontal wellbore. This solution is then modified, using the method of asymptotic matching, to take into account the one-dimensional plane flow and the local increase in the effective hydraulic resistance of the reservoir due to the convergence of the flow into the wellbore. The modified external solution is coupled with the flow across the ICD and the one-dimensional flow inside its basepipe through the pressure/flux continuity conditions at the ICD boundaries. Finally, the resulting singular integro-differential equation is rewritten in dimensionless form and solved numerically for the given total production rate or pressure drawdown, specified at the toe or heel of the wellbore.

This paper is structured as follows. The general formulation of the problem is given in § 2. It includes the description of the ICD design, the main assumption and equations with boundary conditions.

The reservoir flow model is discussed in § 3, where the concept of flow structuring is presented. A similar approach was used in the past for the modelling of the flow performance of a fractured well with a partially penetrating hydraulic fracture [18].

In § 4, the coupling of the reservoir flow with the flow inside the ICD basepipe is described. This leads to a boundary integral equation for the flux along the wellbore as a function of the total production rate. If the flux is found, the pressure around the horizontal wellbore, across the ICD and along the basepipe can be calculated.

The dimensional analysis of the integral equation is presented in § 5, allowing us to reduce the number of parameters.

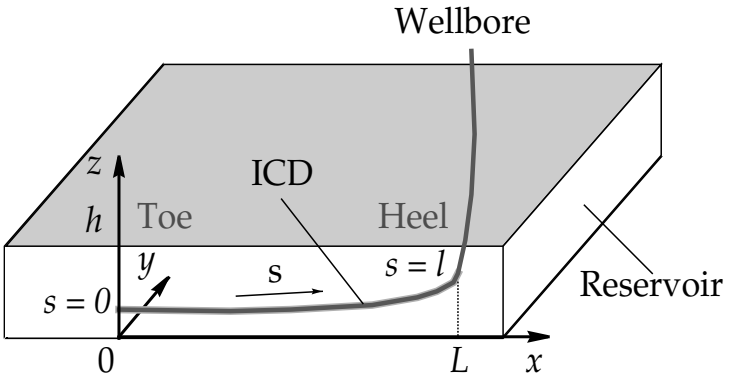

FIGURE 1. Schematic of well with ICD installed in the horizontal section.

In § 6, the numerical method used is presented. It is based on a special quadrature formula for singular integrals with Cauchy type kernels [10]. This quadrature formula allows one to reduce the problem to a system of nonlinear algebraic equations, which can be solved by standard inversion algorithms, using appropriate linearisation and iterations. The ICD parameters have to be specified for the integral equation and therefore solving the forward problem allows one to estimate the flow performance of a horizontal well completed with a given ICD.

The inverse problem, for the determination of the completion parameters (the diameter of perforations and/or the density of basepipe holes) for a given reservoir drawdown pressure or flux distribution along the horizontal wellbore is discussed in § 7. Two basic situations are considered, which correspond to a given reservoir drawdown and a given production profile. Both allow one to find the ICD properties, such as the density of holes in the basepipe and the hole diameters, for any particular requirements.

A few examples, presented in § 9, illustrate the power of the approach developed and outline the steps to be undertaken to check the validity of this technique.

2 Problem formulation

2.1 General assumptions

Let us consider steady-state flow in a horizontal reservoir of thickness h into a nearly horizontal well of radius r_W. We assume that the reservoir occupies the layer $0 \leqslant z \leqslant h$ with impermeable boundaries $z = 0$ and $z = h$. It may have different vertical and horizontal permeabilities, k_V and k_H. The wellbore lies in the vertical plane $y = 0$, and is specified in the parametric form

$$x = x_W(s), \quad z = z_W(s), \quad 0 \leqslant s \leqslant l, \tag{2.1}$$

where s is the wellbore length measured along the wellbore axis from the toe to the heel, and l is the total length (Fig. 1). We also assume that the reservoir thickness is small compared to the wellbore length, but large compared to the wellbore radius, i.e. $r_W \ll h \ll l$. Lastly, the horizontal well has an openhole completion with an Inflow Control Device (ICD). The ICD lies on the bottom of the wellbore and consists of a wire tightly wrapped

https://doi.org/10.1017/S0956792504005546 Published online by Cambridge University Press

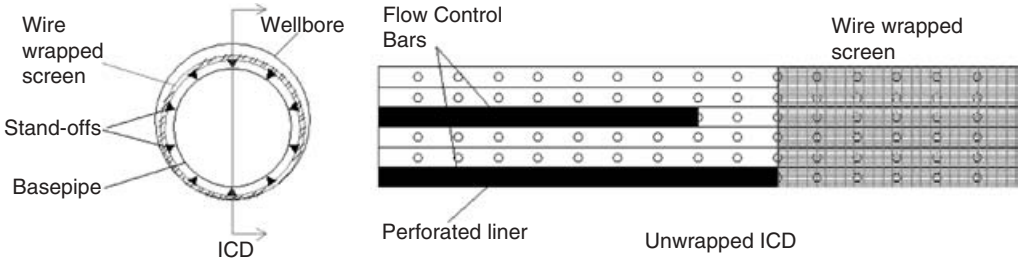

FIGURE 2. Schematic of the ICD design.

around perforated basepipe (Fig. 2). Its purpose is to restrict the flux into the wellbore. The spacing between the external diameter of the ICD and the openhole is assumed to be small; we therefore neglect the axial flow in the annulus conduit. The wellbore pressure is supposed to be uniform in each cross-section of the basepipe and the local pressure drop across the ICD depends on its local hydraulic resistance and the local influx.

2.2 Reservoir flow

Darcy's law for an anisotropic porous medium governs the reservoir flow

$$\mathrm{u}(x,y,z) = -\frac{\mathrm{k}}{\mu}\cdot\nabla p$$
$$\mathrm{k} = \begin{pmatrix} k_H & 0 & 0 \\ 0 & k_H & 0 \\ 0 & 0 & k_V \end{pmatrix} \tag{2.2}$$

where $\mathrm{u}(u_x, u_y, u_z)$ is the flow velocity, and μ is the fluid viscosity.

2.3 Flow across the ICD

The ICD is a device that consists of a wire wrapped around a perforated liner, as shown in Fig. 2. The annular gap between the tubing and the wirescreen is adjusted by some stand-offs, which separate the annulus into several sections evenly distributed around the circumference, the so-called flow paths. Axial rods, slotting in or out of each section between the stand-offs, control the number of open holes in the tubing, providing a simple and easy way to adjust the hydraulic resistance of ICD during installation.

The flow across the ICD is controlled by the pressure difference across the screen and its local hydraulic resistance. For typical production rates from horizontal wells, the screen flow and the annulus flow are supposed to be laminar whereas the flow through perforations is expected to be turbulent. The hydraulic resistance of the perforations controls the pressure drop across the ICD, and therefore

$$\Delta p_D \approx R_P q_W^2, \quad R_P = \frac{8\rho}{\left(\pi d_P^2 C_d N\right)^2}, \quad q_W = 2\pi r_W \bar{u} \tag{2.3}$$

Here N is the density of holes per unit length in the basepipe, d_P is their diameter, ρ is the

https://doi.org/10.1017/S0956792504005546 Published online by Cambridge University Press

fluid density, is $\bar{u}$ the average radial inflow and C_d is the discharge coefficient for suction flow into a pipe through a circular port. The discharge coefficient, C_d, is a function of the parameter $E = 2\Delta p_{ICD}/\rho v^2$, where v is the average axial flow velocity inside the basepipe. It varies in the range 0.45–1.0 with the variation of E between 0.2–100 [13].

2.4 Flow along the wellbore

The average axial flow along the wellbore is governed by the following momentum and continuity equations:

$$\frac{d}{ds}(\rho v^2 A) = -\frac{d}{ds}(PA) + 2\pi r_S \tau, \quad P(s) = p_T(s) - \rho g[z_W(s) - z_W(0)] \tag{2.4}$$

$$\frac{dv}{ds} = \frac{q_W}{A} \tag{2.5}$$

where $A = \pi r_S^2$ is the cross-sectional area of the ICD basepipe, $P(s)$ is the normalised local wellbore pressure, which takes into account the effect of gravity, g, $p_T(s)$ is the pressure inside the basepipe, and $\tau(s)$ is the shear stress produced by friction on the internal walls of the basepipe. The left-hand side of Eq. (2.4) represents the momentum variation due to flow acceleration along the wellbore. It is usually small for flows in horizontal wells compared to the frictional losses and can be neglected (see Appendix A). The shear stress τ can be correlated to the kinetic energy of fluid by the relationship

$$\tau = -C_f \frac{\rho v^2}{2} \tag{2.6}$$

where C_f is the friction factor, which depends on the flow regime (laminar or turbulent), the roughness of the tubing walls, etc., and is usually correlated to the Reynolds number

$$C_f = C_f(\mathrm{Re}), \quad \mathrm{Re} = \frac{2 r_S \rho v}{\mu} \tag{2.7}$$

We will use in this study two simple correlations [11]:

- for the laminar pipe flow

$$C_f = 16\,\mathrm{Re}^{-1}, \quad \mathrm{Re} \leqslant \mathrm{Re}^*; \tag{2.8}$$

- for the turbulent pipe flow

$$C_f = \frac{1}{4}\left(0.0032 + \frac{0.221}{\mathrm{Re}^{0.237}}\right), \quad \mathrm{Re} > \mathrm{Re}^*. \tag{2.9}$$

Here Re^* is the critical Reynolds number, which is in the range 2000–4000, and the transition from laminar to turbulent flow is accompanied by a jump in the friction factor, reflecting the increase in frictional pressure losses in turbulent flow compared to laminar one. Equation (2.8) is equivalent to the Poiseuille solution for the pipe flow and (2.9) is an empirical approximation of the Prandtl law for the turbulent pipe flow given by Nikuradze for smooth pipes [11]. Substituting (2.6) in (2.4) and neglecting the left-hand

https://doi.org/10.1017/S0956792504005546 Published online by Cambridge University Press

side, one has the Darcy–Weisbach equation

$$\frac{dP}{ds} = -\frac{C_f(\mathrm{Re})\rho v^2}{r_S} \tag{2.10}$$

A simple analysis (see Appendix A) shows that, in long enough horizontal wells, the flow inside the well is usually laminar near the toe and turbulent at the heel with the transition occurring somewhere in the middle due to the acceleration of the flow along the wellbore. The pressure gradient dP/ds, in accordance with (2.8) and (2.9), is proportional to the axial velocity $v(s)$ in the laminar flow section of the wellbore and to approximately $v^{1.763}$ at high flow rate when the flow is turbulent. Since the velocity v is proportional to q/A, where q is the flux through the cross-sectional area of the pipe $A = \pi r_S^2$, the pressure gradient dP/ds is proportional to r_S^{-3} for the laminar flow and to $r_S^{-4.536}$ for the turbulent flow inside the ICD basepipe.

2.5 Boundary conditions

There are two sets of boundary conditions: (1) for the flow in the reservoir (the external flow), and (2) for the coupling between the reservoir flow and the flow inside the wellbore through the ICD basepipe (the internal flow).

For the external flow, one has the zero-flux conditions at the top and bottom boundaries of the reservoir:

$$\left.\frac{\partial p}{\partial z}\right|_{z=0} = \left.\frac{\partial p}{\partial z}\right|_{z=h} = 0, \tag{2.11}$$

and the external wellbore pressure at the surface of the openhole interval,

$$p = p_W, \tag{2.12}$$

where the pressure p_W is initially unknown, and has to be determined from the coupling with the internal flow.

Since the reservoir is assumed to be infinite in the horizontal direction, the far field pressure has a logarithmic behaviour at infinity and therefore cannot be specified. The appropriate boundary condition at infinity may be given in terms of the total flow rate from the horizontal wellbore. Because the flow at a large distance from the wellbore has to be radial, one has

$$p = \Pi \log r + \text{const}, \quad \Pi = \frac{\mu q_0}{2\pi h k_H}, \text{ as } \quad r = \sqrt{x^2 + y^2} \to \infty, \tag{2.13}$$

where q_0 is the production rate from the wellbore given by the formula

$$q_0 = \int_0^l q_W(s)\, ds, \quad q_W = 2\pi r_W \bar{u}. \tag{2.14}$$

Here $\bar{u}$ can be expressed in terms of the normal velocity u_n in each cross-section $x = x_W(s)$ as

$$\bar{u}(s) = \int_0^{2\pi} u_n(x_W(s), r_W \cos\varphi, z_W(s) + r_W \sin\varphi) r_W\, d\varphi, \tag{2.15}$$

https://doi.org/10.1017/S0956792504005546 Published online by Cambridge University Press

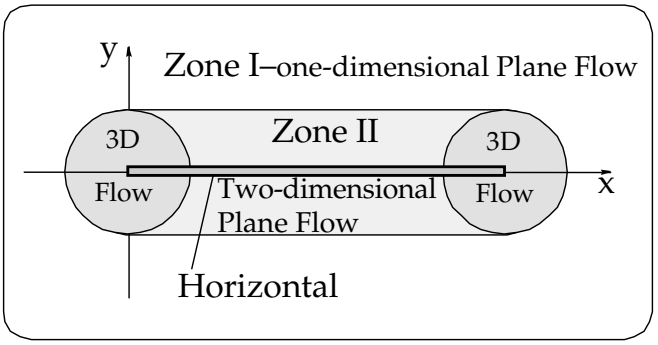

FIGURE 3. The structure of flow pattern around the horizontal wellbore in the reservoir plane.

where we have neglected the slight ellipticity of the wellbore cross-section. The external and internal flows are coupled by the pressure and flux continuity conditions at the wellbore surface

$$p_W = p_T + \Delta p_D, \tag{2.16}$$

$$\frac{dv(s)}{ds} = \frac{q_W(s)}{\pi r_S^2}, \quad v(0) = 0, \tag{2.17}$$

where Δp_D is determined by (2.3), and p_T is the pressure inside the ICD basepipe, which is determined from (2.4) and (2.5).

Equation (2.17) can be integrated to give

$$v(s) = \frac{1}{\pi r_S^2} \int_0^s q_W(\sigma)\, d\sigma. \tag{2.18}$$

3 Reservoir flow model

We exploit below the concept of *flow structuring*, to obtain an approximate solution for the external flow problem. This concept has already been used for the modelling of flow around a partially penetrating hydraulic fracture [13]. The main idea is to simplify the flow pattern around the horizontal well and, using analytical solutions, to reduce the problem dimensionality.

We have already mentioned that the flow should be parallel to the top and bottom of the reservoir at relatively large distances from the horizontal well $\Delta r_F = \sqrt{[x - x_W(s)]^2 + y^2}$, $0 \leqslant s \leqslant l$. The estimate of Δr_F, which takes into account the permeability anisotropy $\omega = \sqrt{k_H/k_V}$, gives the result $\Delta r_F \gg \omega h$. This means that within far field Zone I, shown in Fig. 3, the flow pattern created by the horizontal wellbore is similar to the flow pattern around fully penetrating vertical fractures.

In the internal domain, surrounding the wellbore, and shown in Fig. 3 as Zone II, the flow is almost everywhere locally two-dimensional in each plane $x = \text{const}$, $0 < z < h$, except in the proximity of the toe and the heel, where the flow is purely three-dimensional. We shall, however, neglect these three-dimensional effects, assuming that the flow pattern can be represented by the combination of the flow in Zones I and II.

https://doi.org/10.1017/S0956792504005546 Published online by Cambridge University Press

To obtain the far field pressure induced by the horizontal wellbore, we replace the wellbore by an equivalent vertical fracture. We assume that the fracture is located in the same plane as the horizontal wellbore, $y=0$, and its length, $L=x_W(l)-x_W(0)$, is equal to the projected length of the wellbore on the horizontal plane $z=0$. We also assume that the fracture width is small compared to the reservoir thickness h, but the fracture conductivity is large compared to the reservoir conductivity. Under these assumptions, the pressure inside the fracture, and therefore inside the reservoir, does not depend on z.

If the pressure gradient at the fracture surface is

$$\psi(x)=\left.\frac{\partial p}{\partial y}\right|_{y=0+}, \quad 0<x<L, \tag{3.1}$$

then the pressure induced by the fracture is given by the Poisson integral [1]

$$p(x,y)=\frac{1}{2\pi}\int_0^L \log[y^2+(x-t)^2]\psi(t)\,dt+\text{const.} \tag{3.2}$$

The arbitrary constant will be determined by the specification of the far-field reservoir pressure at some distance from the wellbore, $r_e \gg L$. Bearing this in mind, we will assume below this arbitrary constant to be equal to zero.

Obviously, the parameter $\Pi = r\partial p/\partial r|_{r=\infty}$ is

$$\Pi = \frac{1}{\pi}\int_0^L \psi(t)\,dt. \tag{3.3}$$

The pressure at the fracture surface, which can be identified with the pressure inside the fracture, is given by

$$p_F(x)=\frac{1}{\pi}\int_0^L \log|x-t|\psi(t)\,dt \tag{3.4}$$

and the derivative of pressure variation along the fracture is the principal value integral

$$\frac{dp_F(x)}{dx}=\frac{1}{\pi}\int_0^L \frac{\psi(t)\,dt}{x-t}, \quad 0<x<L. \tag{3.5}$$

The pressure at large distances from the fracture is related to the production rate from the fracture q_0 by

$$p_e \approx \frac{\log r_e}{\pi}\int_0^L \psi(t)\,dt=\frac{\mu q_0 \log r_e}{2\pi h k_H}, \tag{3.6}$$

where q_0 can be expressed in terms of $\psi(x)$ as

$$q_0=2h\frac{k_H}{\mu}\int_0^L \psi(t)\,dt. \tag{3.7}$$

The solution found (3.2) is not valid near the horizontal wellbore (say, $0<x<L$, $|y|\leqslant a\omega h$, $a\approx 3$–5), and it cannot predict correctly the drawdown pressure. To correct the pressure field at the proximity of the wellbore, we now consider the local solution near the horizontal wellbore.

https://doi.org/10.1017/S0956792504005546 Published online by Cambridge University Press

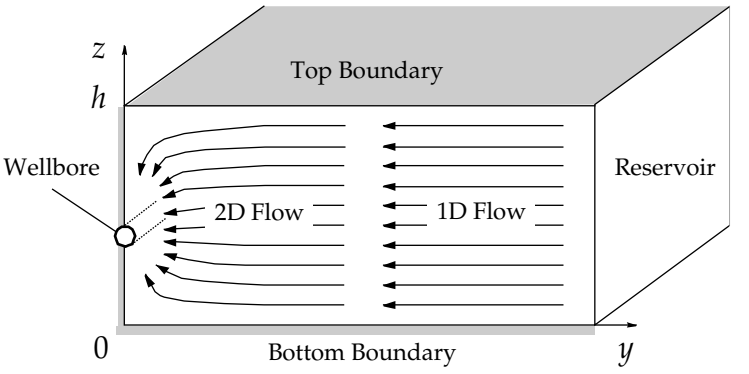

FIGURE 4. The 2D flow near the horizontal wellbore.

The two-dimensional flow near the horizontal wellbore is based on the following assumptions:

1. The deviation of the wellbore trajectory (2.1) from horizontal is small.
2. The pressure variation along the wellbore is slow.
3. The flow near the wellbore is locally along planes $x = \text{const.}$ orthogonal to the horizontal projection of the wellbore trajectory on the vertical plane $y = 0$.

The typical flow pattern in an arbitrary plane $x = x_W(s)$, $0 < s < l$ is shown in Fig. 4. It lies within the bounded strip $\Omega_R(s) = \{-\infty < y < \infty,\ 0 < z < h\}$ with zero-flux boundaries $z = 0$ and $z = h$. Because the plane $x = x_W(s)$ is not perpendicular to the wellbore axis, the cross-sectional area of the wellbore is not circular. Under the assumptions made above, this ellipticity can be neglected. Thus, the pressure $p(y, z)$ has to satisfy the modified Laplace equation in the domain $\Omega_R(s)$:

$$\frac{\partial^2 p}{\partial y^2} + \frac{1}{\omega^2}\frac{\partial^2 p}{\partial z^2} = 0, \quad \omega = \sqrt{\frac{k_H}{k_V}}. \tag{3.8}$$

The zero-flux boundary conditions at the top and bottom of the reservoir are

$$\left.\frac{\partial p}{\partial z}\right|_{z=0} = \left.\frac{\partial p}{\partial z}\right|_{z=h} = 0, \tag{3.9}$$

and the uniform pressure condition along the wellbore wall $\Omega_W(s)$ is

$$p(y, z) = p_W(s), \quad y^2 + [z_W(s) - z]^2 = r_W^2. \tag{3.10}$$

The solution also has the same asymptotic behaviour at a large distance from the wellbore as the pressure field generated by the flow through an equivalent vertical fracture in the plane $x = x_W(s)$. Since we assume that the fluid is incompressible, this condition is equivalent to the matching of the fluxes at infinity ($|y| \to \infty$), where the flow is uniform and parallel to the zero-flux horizontal boundaries $z = 0$ and $z = h$. This means that the pressure behaviour at infinity has to be linear with respect to the distance from the

https://doi.org/10.1017/S0956792504005546 Published online by Cambridge University Press

wellbore:

$$p \approx \psi(x)y + \text{const}, \quad |y| \to \infty. \tag{3.11}$$

Using the fact that the wellbore radius r_W is much smaller than the reservoir thickness h, one can obtain an approximate solution of the problem (3.8)–(3.11) by replacing the wellbore by a point source. The flux generated at infinity is the flux through the wellbore:

$$\left.\frac{\partial p}{\partial y}\right|_{y\to\infty} = \psi(x). \tag{3.12}$$

The solution of the problem (3.8), (3.9) and (3.12) for the point source at $y=0$, $z=z_W(s)$ can be found using the Fourier transform with respect to the coordinate y [1]. The final result is

$$p_L(y,z) = p_S(x)P_L(y,z), \quad p_S(x) = \frac{\omega h}{2\pi}\psi(x) \tag{3.13}$$

$$P_L(y,z) = \log\left\{\cosh\left(\frac{\pi y}{\omega h}\right) + \cos\left[\frac{\pi}{h}(z+z_W-h)\right]\right\} + \log\left\{\cosh\left(\frac{\pi y}{\omega h}\right) - \cos\left[\frac{\pi}{h}(z-z_W)\right]\right\}.$$

The index L is used to emphasise that (3.13) is the local solution for the pressure near the horizontal wellbore.

It is easy to verify that the pressure at the wellbore surface, which corresponds to the approximate solution (3.13), is not uniform: $p_W(s)$ is equal to the pressure, obtained by averaging (3.13) over the wellbore surface $y^2 + [z_W(s) - z]^2 = r_W^2$.

When the wellbore radius r_W is small compared to the reservoir thickness $h(r_W/h \to 0)$, which is usually the case, and the permeability anisotropy is negligible, the non-uniformity in the local pressure at the wellbore surface will be negligible. The problem for highly anisotropic reservoir, $\omega \gg 1$, will however require a special consideration (see Appendix A).

For an arbitrary permeability anisotropy ratio, $0 < \omega < \infty$, the dimensionless pressure at the wellbore, $P_W(s) = p_W(s)/p_S$, found by the method of asymptotic matching under the assumption $\varepsilon = r_W/h \ll 1$, is

$$P_W(s) = \log\left\{1 + \cos\left[\pi\left(\frac{2z_W(s)-h}{h}\right)\right]\right\} + 2\log\left[\frac{\pi\varepsilon(\omega+1)}{2\sqrt{2}\omega}\right]. \tag{3.14}$$

To obtain this result, the solution (3.13) has been refined in the wellbore neighbourhood to satisfy the uniform boundary condition for the pressure along the wellbore surface asymptotically (see details in Appendix A).

Concerning the flux matching at the surface of the fracture, let us assume that the pressure at the wellbore $p_W(s) = p_S P_W(s)$ is known, and then compare the far-field behaviour, given by (3.13), with the local solution for the flow near a fully penetrating fracture (Fig. 5).

The latter does not depend upon the vertical coordinate z, because the flow into the fracture is uniform over the reservoir thickness, and therefore the pressure must vary linearly with the coordinate y

$$p_G(y) = \psi(x)|y|. \tag{3.15}$$

https://doi.org/10.1017/S0956792504005546 Published online by Cambridge University Press

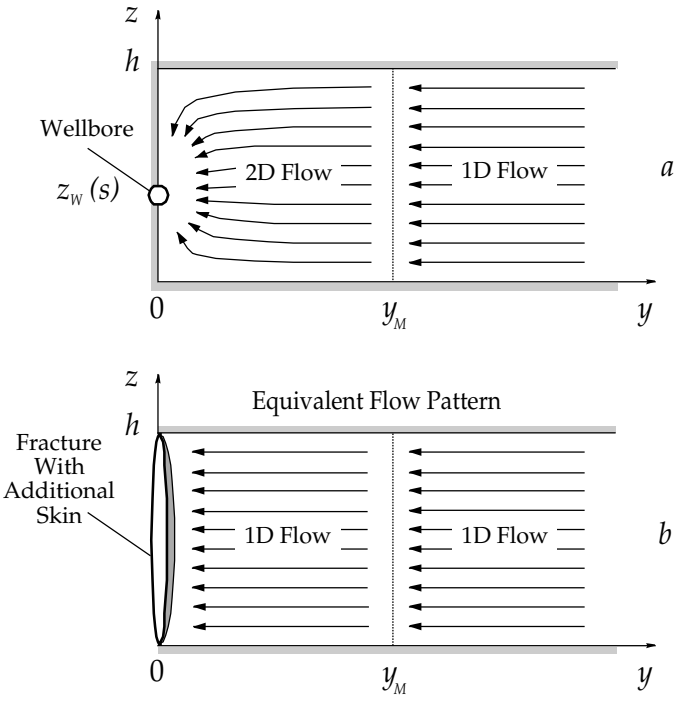

FIGURE 5. The local flow pattern around the horizontal wellbore (a) is replaced by the equivalent flow pattern around the fracture with additional skin (b).

Equation (3.15) is the limit of (3.2) near the fracture surface, having the same behaviour at large y as the solution (3.13).

Considering the flow within the finite domain $|y| \leqslant y_M$, one can find from (3.15) the drawdown pressure over the length $0 \leqslant y \leqslant y_M$,

$$\Delta p_G(y_M) = p_G(y_M) - p_G(0) = \psi(x) y_M, \tag{3.16}$$

where y_M is the parameter through which we match the two flow patterns.

The equivalent pressure drawdown, corresponding to the local flow near the wellbore, can be found from (3.13) as

$$\Delta p_L(y_M, z) = p_L(y_M, z) - p_W(s), \tag{3.17}$$

where the dependence on z disappears with increasing y_M.

The difference between the drawdown pressures (3.17) and (3.16) is

$$\Delta p_F(y_M) = \Delta p_L(y_M) - \Delta p_G(y_M), \tag{3.18}$$

which is the additional pressure drop required to equalise the local influx into the wellbore with the local flux into the equivalent fracture.

To eliminate the dependence of (3.18) on y_M, one can find the asymptotic value of the pressure drop $\Delta p_F(y_M)$ as $y_M \to \infty$:

$$\Delta p_F(x) = -p_W(s) - \frac{\omega h \log 2}{\pi} \psi(x). \tag{3.19}$$

https://doi.org/10.1017/S0956792504005546 Published online by Cambridge University Press

It can be proved that $p_W(s)$ is negative, and the additional pressure drop Δp_F is always positive. From (3.13), $p_W(s)$ is proportional to $\psi(x)$, and therefore $\Delta p_F(x)$ can be represented as

$$\Delta p_F(x) = \Pi_F(x)\psi(x), \quad \Pi_F(x) = -\frac{\omega h}{\pi}\left[\frac{1}{2}P_W(s) + \log 2\right], \tag{3.20}$$

where $P_W(s) = p_W(s)/p_S$ is given by (3.14).

We note that this additional pressure drop, Δp_F, which is required to equate the local hydraulic resistances for the two flow patterns shown in Fig. 5, can be represented in the one-dimensional flow around the fracture as additional 'skin' along the fracture surface. This allows one to preserve the dimensionality of the external solution, taking into account the three-dimensional features of the problem in the boundary conditions only.

The additional pressure drop found above allows one to significantly simplify the solution for the flow inside the reservoir. Indeed, instead of solving the three-dimensional problem for the flow around the horizontal wellbore, one can use the two-dimensional solution for the equivalent fracture (3.2)–(3.4), corrected by $\Delta p_F(x)$ given in (3.20). This means that the external solution for the reservoir pressure at the fracture surface (3.4) has to be replaced by

$$p_F(x) = \frac{1}{\pi}\int_0^L \log|x-t|\psi(t)\,dt - \Delta p_F(x), \quad 0 \leqslant x \leqslant L, \tag{3.21}$$

and therefore, instead of (3.5), one has

$$\frac{dp_F(x)}{dx} = \frac{1}{\pi}\int_0^L \frac{\psi(t)\,dt}{x-t} - \frac{d\Delta p_F(x)}{dx}, \quad 0 < x < L. \tag{3.22}$$

4 Coupling of flow inside the reservoir with flow along the wellbore

The flow inside the ICD basepipe is governed by (2.10) and (2.18), which can be rewritten, using the last relationship in (2.4), as

$$\frac{dp_T}{ds} = -\frac{C_f \rho v^2}{r_S} + \rho g \frac{dz_W}{ds}(s), \tag{4.1}$$

$$v(s) = \frac{1}{\pi r_S^2}\int_0^s q_W(\sigma)\,d\sigma. \tag{4.2}$$

The cross-sectional flux $q_W = 2\pi r_W \bar{u}$ can also be expressed in terms of the external flux at the surface of the equivalent fracture as

$$q_W(s) = \frac{2hk_H}{\mu}\psi(x)|_{x=x_W(s)}. \tag{4.3}$$

It is convenient to represent $C_f(\mathrm{Re})$ as

$$C_f(\mathrm{Re}) = \mathrm{Re}^{-1} f(\mathrm{Re}), \quad \mathrm{Re} = \frac{2r_S \rho v}{\mu}, \tag{4.4}$$

where the function $f(\mathrm{Re})$ takes into account the dependence of $C_f(\mathrm{Re})$ on the flow regime.

https://doi.org/10.1017/S0956792504005546 Published online by Cambridge University Press

Substituting (4.4) into (4.1), one obtains

$$\frac{dp_T}{ds} = -\frac{f(\mathrm{Re})\mu v(s)}{2r_S^2} + \rho g \frac{dz_W}{ds}(s), \quad \mathrm{Re} = \frac{2r_S \rho v(s)}{\mu}. \tag{4.5}$$

For a laminar flow inside the ICD basepipe, $\mathrm{Re} \leqslant \mathrm{Re}^*$, (4.5) gives a linear relationship between the pressure derivative along the wellbore and the flow velocity. This relationship, however, becomes nonlinear when the transition from a laminar to turbulent flow occurs.

Equations (4.2) and (4.6) determine the internal solution, which now has to be coupled with the reservoir flow.

The external flow inside the reservoir and the internal flow inside the wellbore are connected by the ICD. The continuity of fluxes is guaranteed by (4.2) with $q_W(s)$ determined by (4.3). The pressure drop across the ICD is given by (2.3):

$$\Delta p_D(s) = R_p(s) q_W^2(s), \tag{4.6}$$

and it has to satisfy (2.16) with p_W replaced by p_F, determined in (3.21), i.e.

$$p_F(x)|_{x=x_W(s)} = p_T(s) + \Delta p_D(s), \tag{4.7}$$

hence

$$p_F(x) = [p_T(s) + \Delta p_D(s)]_{x=x_W(s)}. \tag{4.8}$$

We can differentiate (4.8) with respect to x, and then it will be sufficient to require that (4.8) is satisfied at $x = s = 0$ only. Finally, we have

$$\frac{dp_F(x)}{dx} = \frac{1}{x'_W(s)} \left[\frac{dp_T(s)}{ds} + \frac{d\Delta p_D(s)}{ds} \right]_{x=x_W(s)}, \tag{4.9}$$

$$p_F(0) = p_T(0) + \Delta p_D(0). \tag{4.10}$$

Finally, substituting (3.22), (4.5) and (4.6) in (4.9) and using (4.2) and (4.3), we arrive at a nonlinear integro-differential equation for the function $\psi(x)$ in the interval $0 < x < L$:

$$\frac{1}{\pi} \int_0^L \frac{\psi(t)\,dt}{x-t} - \frac{d}{dx}[\Pi_F(x)\psi(x)] + a_1(x) \int_0^x \frac{\psi(t)\,dt}{b_1(t)} = a_2 \frac{d}{dx}[b_2(x)\psi^2(x)] + a_3(x), \tag{4.11}$$

where

$$\Pi_F(x) = -\frac{\omega h}{\pi} \left[\frac{1}{2} P_W(s) + \log 2 \right],$$

$$a_1(x) = \left. \frac{f(\mathrm{Re}) h k_H}{\pi r_S^4 \frac{dx_W}{ds}(s)} \right|_{x=x_W(s)}, \quad b_1(t) = \left. \frac{dx_W(\sigma)}{d\sigma} \right|_{t=x_W(\sigma)},$$

$$a_2 = \left(\frac{2hk_H}{\mu} \right)^2, \quad b_2(x) = R_p(s)|_{x=x_W(s)},$$

$$a_3(x) = \rho g \left. \frac{dz_W(s)}{dx_W(s)} \right|_{x=x_W(s)}. \tag{4.12}$$

https://doi.org/10.1017/S0956792504005546 Published online by Cambridge University Press

The nonlinearity is caused by the function $a_1(x)$ when the flow in the basepipe is turbulent, and by the first term in the right-hand side of the equation, representing the pressure drop across the ICD.

Equation (4.11) has to be closed with the normalisation condition (3.7), which specifies the production rate from the horizontal wellbore:

$$\int_0^L \psi(x)\,dx = \frac{\mu q_0}{2hk_H}. \tag{4.13}$$

Equations (4.11), (4.13) can now be used for two purposes:

- The forward problem for the determination of the function $\psi(x)$, which determines the production profile from the horizontal wellbore with or without ICD.
- The inverse problem for the determination of the ICD properties (the density of holes in the basepipe, N, and the hole diameter, d_P, along the wellbore) for a specified reservoir drawdown pressure along the wellbore or the production profile.

5 Dimensional analysis

The integro-differential equation (4.12) and the normalisation condition (4.14) can be rewritten in the dimensionless forms:

$$\int_0^1 \frac{\Psi(T)\,dT}{X-T} - \frac{d}{dX}(\Omega\Psi) + A_1 \int_0^X \frac{\Psi(T)\,dT}{B_1(T)} = A_2 \frac{d}{dX}(B_2\Psi^2) + A_3, \quad 0 < X < 1, \tag{5.1}$$

$$\int_0^1 \Psi(X)\,dX = 1, \tag{5.2}$$

where

$$X = \frac{x}{L}, \quad \Psi(X) = \frac{2hk_HL}{\mu q_0}\psi, \quad \Omega(X) = -\frac{\omega h}{L}\left[\frac{1}{2}P_W(s) + \log 2\right]_{X=x_W(s)/L},$$

$$A_1(X) = \left.\frac{f(\mathrm{Re})hk_HL}{r_S^4 \dfrac{dx_W}{ds}(s)}\right|_{X=x_W(s)/L}, \quad B_1(X) = \left.\frac{dx_W}{ds}(s)\right|_{X=x_W(s)/L}$$

$$A_2 = \frac{16hk_H\rho q_0}{\pi\mu d_P^4 M^2}, \quad B_2(X) = (C_dN_S)^{-2}, \quad A_3(X) = \left.\frac{2\pi hk_HL\rho g}{\mu q_0}\,\frac{dz_W(s)}{dx_W(s)}\right|_{X=x_W(s)/L}, \tag{5.3}$$

$$M = \frac{L}{L_S}, \quad N_S(X) = NL_S.$$

Here L_S is the length of a single ICD section, M is the total number of ICD sections installed and N_S is the number of holes in the basepipe of an ICD section. Although N_S varies discretely with X (from section to section), we shall assume for the time being that $N_S(X)$ is a continuous function of the dimensionless coordinate X.

Let us estimate the parameters involved in (5.1) for the typical data:

Production rate $q_0 = 10^3\ \mathrm{m}^3/\mathrm{day}$
Wellbore length $l = 300\ \mathrm{m}$

https://doi.org/10.1017/S0956792504005546 Published online by Cambridge University Press

Wellbore radius	$r_W = 0.10\,\text{m}$
Reservoir thickness	$h = 10\,\text{m}$
Horizontal permeability	$k_H = 100\,\text{mD}$
Vertical permeability	$k_V = 100\,\text{mD}$
Fluid viscosity	$\mu = 1\,\text{cp}$
Fluid density	$\rho = 1000\,\text{kg/m}^3$
Gravity	$g = 9.8\,\text{m/s}^2$
Internal radius of ICD basepipe	$r_S = 0.03\,\text{m}$
Length of ICD section	$L_S = 3.66\,\text{m}$
Diameter of holes in ICD tubing	$d_P = 0.002\,\text{m}$.

We also assume for simplicity that the wellbore is purely horizontal and located in the middle of the reservoir pay-zone, i.e.

$$x_W(s) = s, \quad \frac{dx_W(s)}{ds} = 1, \quad z_W(s) = h/2, \quad \frac{dz_W(s)}{ds} = 0 \quad \text{and} \quad L = l.$$

For these data, one obtains $\Omega \approx 0.1$ and $A_2 \approx 0.3$. If the flow is laminar $A_1 \approx 5 \cdot 10^{-5}$, and it is independent of the production rate. For the turbulent case, A_1 depends upon the production rate through the Reynolds number:

$$\text{Re}_{\max} = \frac{2r_S \rho v_{\max}}{\mu} = \frac{2\rho q_0}{\pi r_S \mu}. \tag{5.4}$$

Thus, for the production rate $q_0 = 1000\,\text{m}^3/\text{day}$, we have $\text{Re}_{\max} \approx 2.7 \cdot 10^5$ and $A_1 \approx 0.37$. The parameter A_1 is responsible for the frictional pressure losses along the wellbore and, as one can see, these pressure losses are not negligible. Furthermore, we shall see that they are usually comparable to the pressure drop in the reservoir and across the ICD.

It also follows from (5.3) that the diameter of holes in the ICD basepipe, d_P, can have a significant effect on the ICD flow performance because $A_2 \propto d_P^{-4}$, as can the number of holes in each ICD section, N_S, since $B_2 \propto N_S^{-2}$.

6 Numerical method for the forward problem

To illustrate the numerical method, consider the linear equation

$$\int_0^1 \frac{\Psi(T)\,dT}{X - T} - \frac{d}{dX}(\Lambda\Psi) + \Gamma(X)\int_0^X \Psi(T)\,dT = \Phi(X), \quad 0 < X < 1, \tag{6.1}$$

which, together with the normalisation condition (5.2), can be solved by Lifanov's method [10], which is based on a special quadrature formula for singular integrals.

This method requires the two sets of nodes in the interval $0 \leqslant X \leqslant 1$,

$$\begin{aligned} X_i &= i\Delta X, \quad \Delta X = \frac{1}{n+1}, \quad i = 1, 2, \ldots, n, \\ X_{i0} &= X_i + \frac{\Delta X}{2}, \quad i = 1, 2, \ldots, n-1, \end{aligned} \tag{6.2}$$

https://doi.org/10.1017/S0956792504005546 Published online by Cambridge University Press

where n is the number of nodes $X = X_i$ in the interval $0 \leqslant X \leqslant 1$, where the unknown function $\Psi_i = \Psi(X_i)$ has to be found.

One obtains the equations for Ψ_i by substituting $X = X_{i0}$ for $i = 1, 2, \ldots, n-1$ into (6.1) and using the normalisation condition (5.2) as the last equation. Replacing integrals by finite sums, which are calculated using the values of integrand expressions at the points $T = X_j$, we arrive at the linear algebraic equations:

$$\sum_{j=1}^{n} \frac{\Psi_j}{X_{i0} - X_j} \Delta X - \frac{\Lambda(X_{i+1})\Psi_{i+1} - \Lambda(X_i)\Psi_i}{\Delta X} + \Gamma(X_{i0}) \sum_{j=1}^{i} \Psi_j \Delta X = \Phi(X_{i0}), \quad i = 1, 2, \ldots, n-1,$$
$$\sum_{j=1}^{n} \Psi_j \, \Delta X = 1, \tag{6.3}$$

which can be solved by the Gauss method with partial pivoting.

When $\Lambda \neq 0$ and $\Gamma(X)$ is constant as $X \to 0$, The asymptotic form of the solution of (6.1) near the end $x = 0$ can be shown to be of the form

$$\Psi(X) = A(-|\Lambda| + X \ln X) + BX + \ldots, \tag{6.4}$$

which can be checked by direct substitution in (6.1), the constants A and B being determined by from a full numerical solution. The numerical method has been tested for the simplified linear equation

$$\int_0^1 \frac{\Psi(T)\, dT}{X - T} = 0, \quad 0 < X < 1; \quad \int_0^1 \Psi(X)\, dX = 1, \tag{6.5}$$

having the analytical solution

$$\Psi(X) = \frac{2}{\pi}[1 - (2X - 1)^2]^{-1/2}, \tag{6.6}$$

which is more singular than (6.4). The results of calculations of the function

$$F(X) = \frac{\pi}{2}[1 - (2X - 1)^2]^{1/2} \Psi(X), \tag{6.7}$$

which should be 1 everywhere in the interval $0 \leqslant X \leqslant 1$, are shown in Fig. 6 for $n = 100$, 200, 300, 400, 500 and 600. Even in this worst case, where the function is singular at both ends, the numerical method gives accurate numerical results for $\int_0^X \Psi(T)\, dT$, although $\Psi(T)$ is of necessity inaccurate near the ends. Hence, we conjecture that for the full problem ($\Lambda \neq 0$) our numerical method is sufficiently accurate.

The nonlinearity of (5.1) requires us to solve the system (6.3) iteratively, and update the coefficients $\Lambda(X_i)$ and $\Gamma(X_{i0})$ at each iteration.

7 Inverse problem

For the inverse problems, one of the functions $\Delta p_R(x) = p_e - p_F(x)$ or $\psi(x)$ is specified, and one has to find the number of holes in each ICD section, $N_S(x)$, and their diameter,

https://doi.org/10.1017/S0956792504005546 Published online by Cambridge University Press

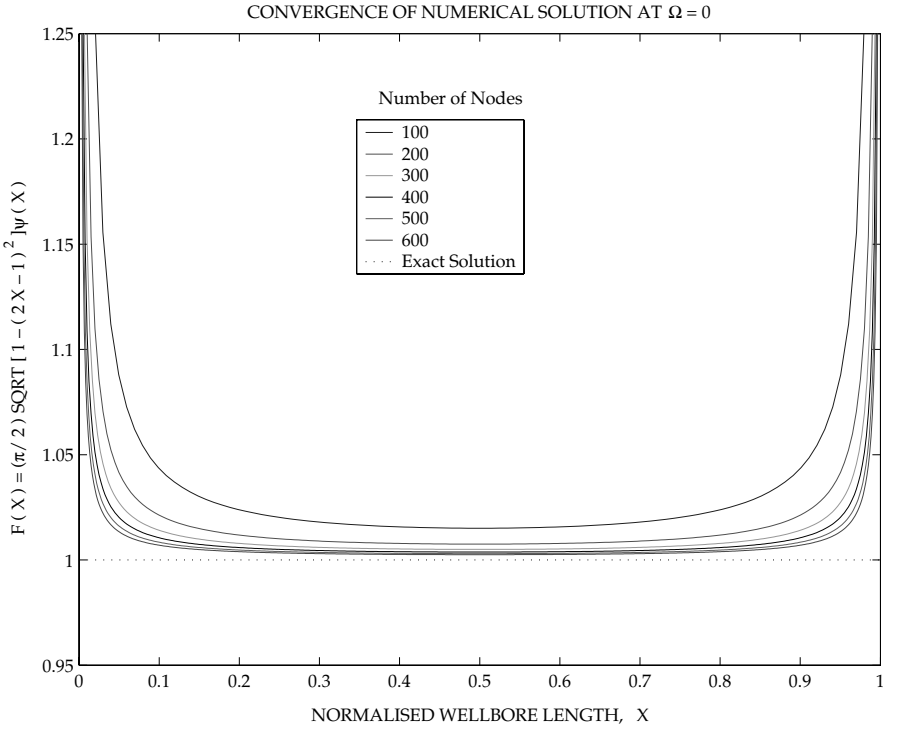

FIGURE 6. The convergence analysis of the numerical solutions at $\Omega = 0$ versus the number of nodes, n, in the interval $0 \leqslant X \leqslant 1$.

d_P. If the diameter d_P is predefined then the density of holes per ICD section, $N_S(x)$, is the only ICD property to be determined.

7.1 Uniform reservoir drainage

Let us consider first the important inverse problem, which corresponds to the ICD tuning with the goal to achieve uniform reservoir drawdown along the horizontal wellbore $\Delta p_R(x) = \Delta p_{R0} = \text{const}$, i.e.

$$p_e - p_F(x) = \Delta p_{R0}, \tag{7.1}$$

where $p_F(x)$ is the pressure at the wellbore wall (i.e. at the external boundary of the ICD), and p_e is the far field reservoir pressure, calculated at some distance from the wellbore. The pressure $p_F(x)$ is related to the flux through the wellbore, determined by the function $\psi(x)$, by (3.22) and (3.20), which can be combined together to the equation

$$\frac{dp_F(x)}{dx} = \frac{1}{\pi}\int_0^L \frac{\psi(t)\,dt}{x-t} - \frac{d}{dx}[\Pi_F(x)\psi(x)], \quad 0 < x < L, \tag{7.2}$$

which does not depend upon any ICD properties. Substituting (7.1) into (7.2), one obtains

$$\frac{1}{\pi}\int_0^L \frac{\psi(t)\,dt}{x-t} - \frac{d}{dx}[\Pi_F(x)\psi(x)] = 0, \quad 0 < x < L. \tag{7.3}$$

https://doi.org/10.1017/S0956792504005546 Published online by Cambridge University Press

As above, this equation has to be complemented with the normalisation condition (4.14):

$$\int_0^L \psi(x)\,dx = \frac{\mu q_0}{2hk_H}. \tag{7.4}$$

Using the dimensionless variables (5.3), (7.3) and (7.4) can be represented in the dimensionless form

$$\int_0^1 \frac{\Psi(T)\,dT}{X-T} - \frac{d}{dX}(\Omega\Psi) = 0, \quad 0 < X < 1; \quad \int_0^1 \Psi(X)\,dX = 1. \tag{7.5}$$

Problem (7.5) has to be solved before the calibration of the ICD properties. The solution $\Psi(X)$ depends upon a single dimensionless function, $\Omega(X)$, which combines all the reservoir/wellbore parameters affecting the reservoir flow. In accordance with (5.3), one has

$$\begin{gathered}\Omega(X) = -\frac{\omega h}{L}\left[\frac{1}{2}P_W(s) + \log 2\right]_{X=x_W(s)/L},\\ P_W(s) = \log\left\{1 + \cos\left[\pi\left(\frac{2z_W(s)-h}{h}\right)\right]\right\} + 2\log\left[\frac{\pi\varepsilon(\omega+1)}{2\sqrt{2}\omega}\right],\end{gathered} \tag{7.6}$$

where $\varepsilon = r_W/h$ is the dimensionless wellbore radius. In the simplest situation, when the wellbore is parallel to the reservoir boundaries, we have $z_W(s) = \text{const}$ and $x_W(s) = s$. In this case, the dependence on the parameter s disappears, $\Omega(X)$ becomes uniform along the wellbore, and $\Psi(X)$ depends upon a single parameter Ω. Due to its importance, this solution is computed in Fig. 10 for Ω varying in a wide range.

Equation (5.1) can thus be represented in a simplified form:

$$A_1\int_0^X \frac{\Psi(T)\,dT}{B_1(T)} = \frac{d}{dX}(B_3\Psi^2) + A_3, \quad 0 < X < 1, \tag{7.7}$$

where

$$\begin{gathered}A_1(X) = \left.\frac{f(\mathrm{Re})hk_HL}{r_S^4\dfrac{dx_W}{ds}(s)}\right|_{X=x_W(s)/L}, \quad B_1(X) = \left.\frac{dx_W}{ds}(s)\right|_{X=x_W(s)/L}\\ B_3 = A_2B_2 = \frac{B}{\left(d_P^2\,N_S\right)^2}, \quad B = \frac{16hk_H\rho q_0}{\pi\mu M^2C_d^2}, \quad A_3(X) = \left.\frac{2\pi hk_HL\rho g}{\mu q_0}\,\frac{dz_W(s)}{dx_W(s)}\right|_{X=x_W(s)/L}.\end{gathered} \tag{7.8}$$

In (7.7), the first term on the LHS represents the frictional pressure losses along the basepipe, whilst the first term on the RHS represents the pressure drop across the ICD and the last term is the gravity effect. Thus, the ICD calibration has to equalise the frictional pressure losses along the basepipe with the pressure drop across the ICD. If the horizontal wellbore is not parallel to the reservoir boundaries, the small contribution into this balance, A_3, is attributed to the gravity effect.

The ICD properties to be tuned are only involved in the parameter B_3, wherein the parameter N_P characterises the open for flow area of the ICD basepipe section. Let us

https://doi.org/10.1017/S0956792504005546 Published online by Cambridge University Press

consider as an example the case $B_1 = 1, A_3 = 0$. We shall neglect for simplicity the slight dependence of the discharge coefficient C_d on the flow rate through the basepipe and the pressure drop across the ICD, involved in the parameter $E = 2\Delta p_{ICD}/\rho v^2$ (see Folefac *et al.* [6]). Assuming that $\Psi(X)$, and therefore $A_1(X)$ are known, and integrating (7.7), we obtain the following equation for the unknown parameter $B_3(X)$:

$$\int_0^X A_1(\Theta) \int_0^\Theta \Psi(T)\, dT\, d\Theta = B_3(X)\Psi^2(X), \quad B_3(X) = \frac{B}{N_P^2(X)}. \tag{7.9}$$

The left-hand side of (7.9) tends to zero as $X \to 0$, and therefore if $B_3(0) = 0$ or $N_P(0) = \infty$, i.e. the ICD hydraulic resistance at the toe of the horizontal wellbore has to vanish. This result reflects the fact that there are no frictional pressure losses at the very end of the toe of the horizontal wellbore, and therefore there should not be any flow restrictions for the influx into the wellbore.

When $\Omega = 0$, the flux $\Psi(X)$ is given by (6.5), and therefore has the following asymptotic behaviour at $X \to 0$:

$$\Psi(X) \sim \frac{1}{\pi\sqrt{X}}, \quad X \to 0. \tag{7.10}$$

Substituting (7.10) into (7.9) and integrating its left-hand side, we have

$$\frac{4A_1}{3\pi} X^{3/2} = \frac{B}{\pi^2 N_P^2(X)} X^{-1}, \tag{7.11}$$

i.e.

$$N_P(X) \sim C_I X^{-5/4}, \quad C_I = \sqrt{\frac{3B}{4\pi A_1}}, \quad X \to 0. \tag{7.12}$$

Similarly, it can be shown that, at the heel of the horizontal wellbore, $X = 1$, where the frictional pressure losses along the basepipe are finite, $N_P(X)$ is also singular:

$$N_P(X) \propto \Psi(X) \sim \sqrt{1 - X}, \quad X \to 1, \tag{7.13}$$

when $\Omega > 0$. In this case, the flux $\Psi(X)$ is finite at the both ends of the wellbore, and therefore

$$\Psi(X) \sim \Psi_0 = \text{const.}, \quad X \to 0. \tag{7.14}$$

Using (7.9), we arrive at the relationship

$$N_P(X) \sim C_{II} X^{-1}, \quad C_{II} = \sqrt{\frac{2B\Psi_0}{A_1}}, \quad X \to 0. \tag{7.15}$$

There is no singularity in $N_P(X)$ behaviour at $X = 1$ because, in this case, $\Psi(X)$ is finite everywhere and $N_P(X) \propto \Psi(X)$ at $X \to 1$.

Another interesting result, which follows from (7.6)–(7.9), is the effect of the production rate, q_0, on the hole density, N_S, or the combined parameter $N_P = d_P N_S$. This effect is nonlinear due to nonlinearity of the friction factor $C_f(\mathrm{Re})$ for a turbulent flow through the basepipe. Indeed, the Reynolds number along the basepipe, which can be

https://doi.org/10.1017/S0956792504005546 Published online by Cambridge University Press

expressed as

$$\mathrm{Re} = \frac{2\rho q_0}{\pi r_S \mu} \int_0^X \Psi(X)\, dX, \tag{7.16}$$

is proportional to the production rate q_0, and therefore, in accordance with (4.5) at $\mathrm{Re} > \mathrm{Re}^*$, one has

$$f(\mathrm{Re}) = \mathrm{Re} C_f(\mathrm{Re}) \propto q_0^{0.763}. \tag{7.17}$$

This means that the two parameters, A_1 and B in (7.9) behave as follows:

$$A_1 \propto q_0^{0.763}, \quad B \propto q_0, \quad \mathrm{Re} > \mathrm{Re}^*, \tag{7.18}$$

and therefore one finally has

$$N_P \propto q_0^{\alpha}, \quad \alpha \approx 0.12. \tag{7.19}$$

Hence, the dependence of the hole density on the production rate should be weak.

7.2 Specified production profile

In another inverse problem of ICD calibration, the function $\Psi(X)$ is supposed to be specified in such a way that it satisfies the normalisation condition (5.2), and (5.1) has to be used to determine N_P such that $N_P(X) = d_P^2 N_S$. Hence

$$\int_0^1 \frac{\Psi(T)\, dT}{X - T} - \frac{d}{dX}(\Omega\Psi) + A_1 \int_0^X \frac{\Psi(T)\, dT}{B_1(T)} = B \frac{d}{dX}\left(\frac{\Psi}{N_P}\right)^2 + A_3, \quad 0 < X < 1, \tag{7.20}$$

so that

$$\left[B \frac{\Psi^2(T)}{N_P^2(T)}\right]_{T=0}^{T=X} = \int_0^1 \log\left|\frac{X - T}{T}\right| \Psi(T)\, dT - [\Omega(T)\Psi(T)]_{T=0}^{T=X} + \int_0^X A_1(\Theta)\, d\Theta \int_0^{\Theta} \frac{\Psi(T)\, dT}{B_1(T)} - A_4(X), \tag{7.21}$$

where

$$B = \frac{16 h k_H \rho q_0}{\pi \mu M^2 C_d^2}, \quad A_4(X) = \frac{2\pi h k_H \rho g}{\mu q_0} [z_W(s) - z_W(0)]_{X = x_W(s)/L}. \tag{7.22}$$

Equation (7.21) can be used for the calculation of the function $N_P(X)$ for the specified $\Psi(X)$. It requires, however, an additional condition for the determination of its boundary value $N_{P0} = N_P(0)$.

Let us consider as an example the uniform flux solution $\Psi(X) = 1$, assuming also that $\Omega(X) = \mathrm{const}$. The gravity term A_4 can be neglected. Then (7.21) can be rewritten in the form

$$\frac{B}{N_P^2(X)} = \frac{B}{N_{P0}^2} + X \log X + (1 - X)\log(1 - X) + \int_0^X A_1(\Theta)\, d\Theta \int_0^{\Theta} \frac{dT}{B_1(T)}. \tag{7.23}$$

https://doi.org/10.1017/S0956792504005546 Published online by Cambridge University Press

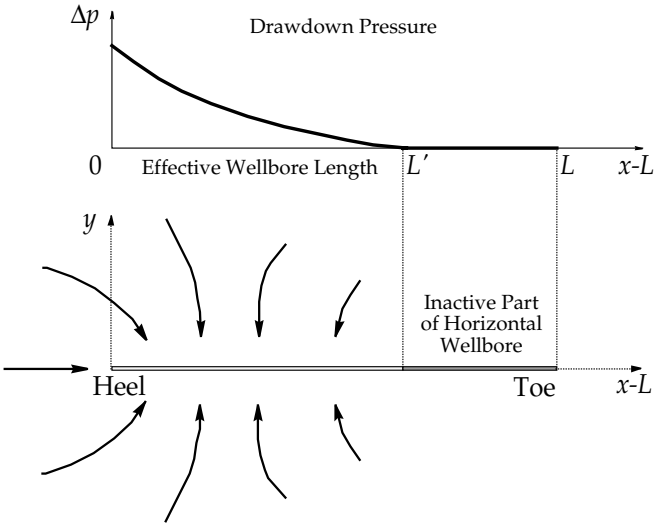

FIGURE 7. Partially producing horizontal wellbore.

It follows from (7.23) that the normalised hole density, $N_P(X)$, is bounded as $X \to 0$. Similarly, for a small $1-X>0$, the variation of $N_P(X)$ is determined by the term $(1-X)\log(1-X)$, and the boundary value is given by the formula

$$\frac{B}{N_P^2(1)} = \frac{B}{N_{P0}^2} + \int_0^1 A_1(\Theta)\,d\Theta \int_0^{\Theta} \frac{dT}{B_1(T)}. \tag{7.24}$$

8 Reservoir drawdown calculations

In all reservoir drawdown calculations, we must remember that *the frictional pressure drop along the basepipe of the horizontal wellbore (from its heel to the toe) cannot exceed the reservoir drawdown pressure at the heel.* The typical situation that may occur is shown in Fig. 7, where the frictional pressure losses inside the basepipe reduce the effective length of the horizontal wellbore.

To satisfy this constraint, one must verify whether the restriction on the drawdown has been reached or not, and if it has been exceeded, reduce the production rate.

Now the reservoir drawdown pressure is determined as

$$\Delta p_R(x) = p_e - p_F(x), \quad 0 \leqslant x \leqslant L, \tag{8.1}$$

where p_e is the pressure at the distance r_e to the middle of the horizontal wellbore along the plane $x = L/2$:

$$p_e = p\left(\frac{L}{2}, r_e\right) = \frac{1}{\pi}\int_0^L \log\sqrt{r_e^2 + \left(\frac{L}{2}-t\right)^2}\,\psi(t)\,dt. \tag{8.2}$$

https://doi.org/10.1017/S0956792504005546 Published online by Cambridge University Press

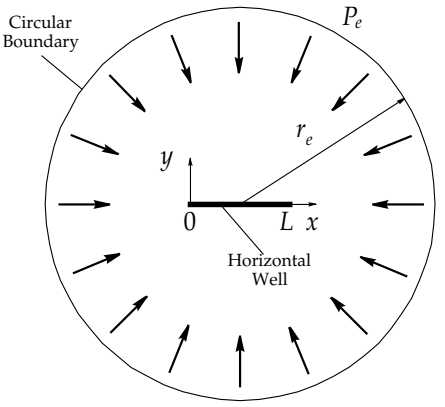

FIGURE 8. The far field radial flow around the horizontal wellbore.

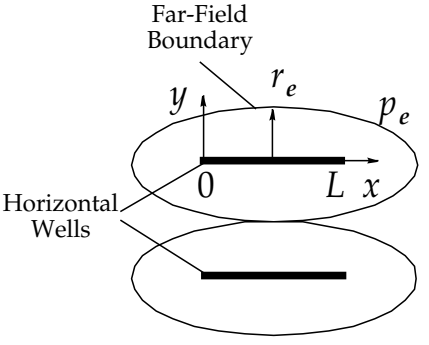

FIGURE 9. The definition of the far-field pressure for neighbouring horizontal wells.

This definition is consistent with that given in (3.6) for a single horizontal wellbore, in a circular reservoir with the radius $r_e \gg L$, as shown in Fig. 8:

$$p_e \sim \frac{\log r_e}{\pi} \int_0^L \psi(t)\, dt = \frac{\mu q_0 \log r_e}{2\pi h k_H}. \tag{8.3}$$

Thus, in all our examples, we use (8.2) as an approximation for parallel horizontal wells when the distances between them are of the order or smaller than their producing lengths. The example of two horizontal wells is shown in Fig. 9. In those cases, the distance to the far field reference point, r_e, can be determined as half of the distance between the wells.

The pressure at the wellbore wall, $p_F(x)$, in accordance with (3.21) and (3.20), is

$$p_F(x) = \frac{1}{\pi} \int_0^L \log|x-t|\psi(t)\, dt - \Pi_F(x)\psi(x), \tag{8.4}$$

and therefore the reservoir drawdown pressure along the wellbore can be expressed by using (8.1) and (8.2) as

$$\Delta p_R(x) = \frac{1}{\pi} \int_0^L \log \frac{\sqrt{r_e^2 + (0.5L - t)^2}}{|x-t|} \psi(t)\, dt + \Pi_F(x)\psi(x), \tag{8.5}$$

https://doi.org/10.1017/S0956792504005546 Published online by Cambridge University Press

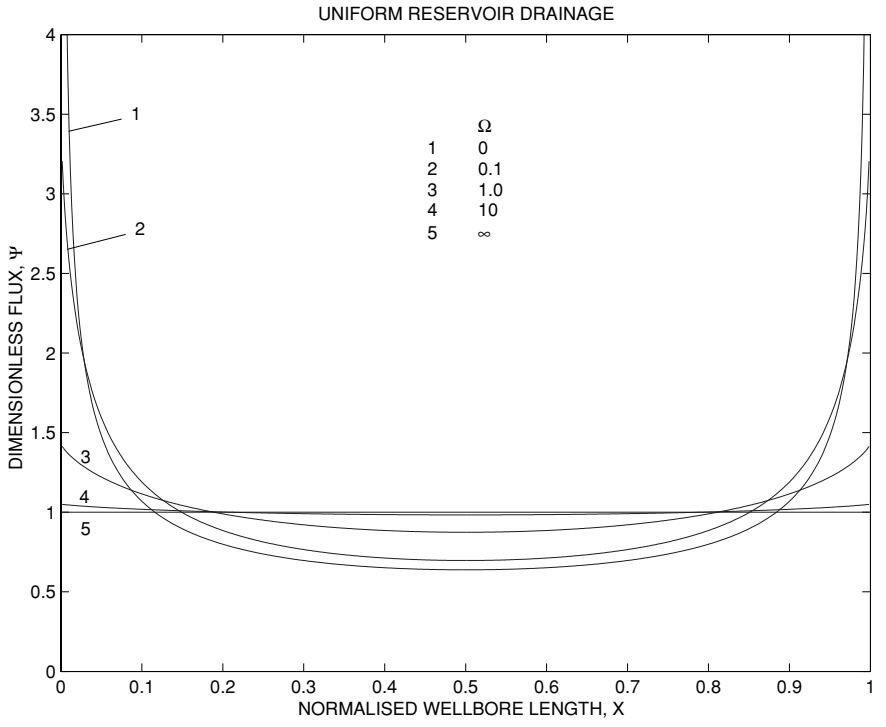

FIGURE 10. Flux along the horizontal wellbore for a uniform wellbore pressure.

or in the dimensionless form

$$\Delta P_R(X) = \frac{2\pi h k_H \, \Delta p_R}{\mu q_0} = \int_0^1 \log \frac{\sqrt{(r_e/L)^2 + (0.5 - T)^2}}{|X - T|} \Psi(T)\, dT + \Omega \Psi(X). \qquad (8.6)$$

9 Examples

9.1 Uniform pressure drawdown

9.1.1 *Forward problem – flux calculation*

The calculations have been carried out for a uniform Ω along the wellbore length ($0 \leqslant X \leqslant 1$) for 600 nodes. The results, $\Psi(X)$, are shown in Fig. 10 for $\Omega = 0, 0.1, 1.0, 10$ and ∞.

When Ω is small, $\Psi(X)$ is close to the analytical solution (6.5), corresponding to $\Omega = 0$. This solution represents the situation when the horizontal wellbore behaves like a vertical fracture of infinite conductivity, and therefore can be considered as an approximation for the case of a very large wellbore radius.

The behaviour of the numerical solution at small Ω is demonstrated in Fig. 11, where the function $F(X)$, determined in (6.6), is plotted. One can see that the numerical solution at $\Omega = 0.001$ becomes very close to the numerical solution, corresponding to $\Omega = 0$. These calculations have been carried out for 600 nodes.

https://doi.org/10.1017/S0956792504005546 Published online by Cambridge University Press

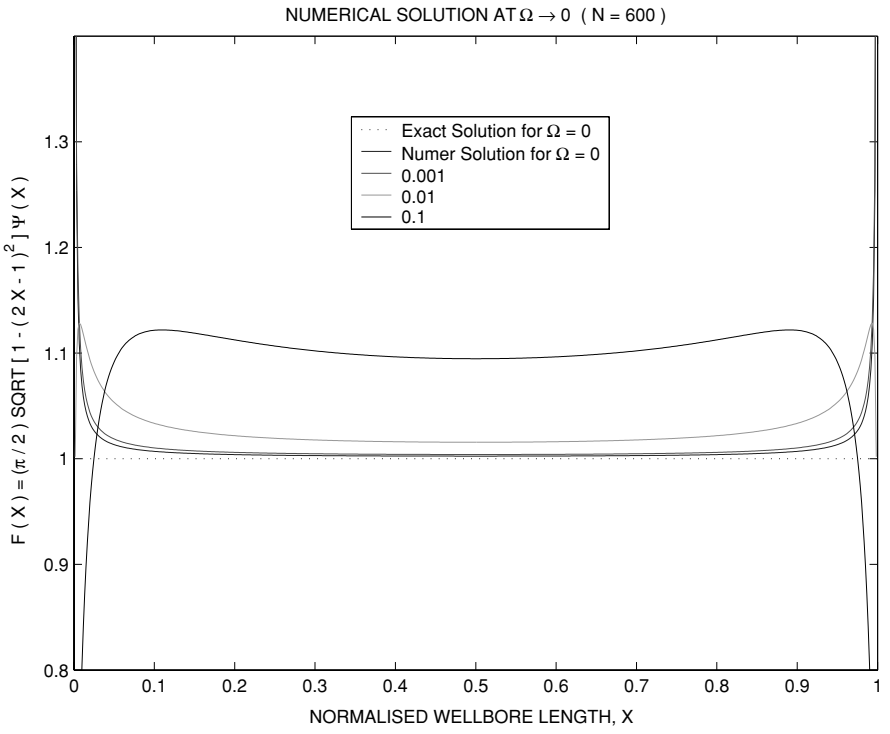

FIGURE 11. The behaviour of the numerical solution at small Ω in the case of uniform reservoir drainage.

9.1.2 *Productivity of horizontal well*

The productivity of the wellbore is usually characterised by its productivity index

$$\Lambda_0 = q_0/\Delta p_{R0}, \tag{9.1}$$

and its productivity ratio

$$I_0 = \Lambda_0/\Lambda, \tag{9.2}$$

where q_0 is the production rate, Δp_{R0} is the pressure drawdown and Λ is the reference productivity index, which is used for comparison. In our case,

$$\Lambda = \Lambda_F = \frac{2\pi h k_H}{\mu \log(r_e/r_0)}, \quad r_0 = \frac{L}{4}, \tag{9.3}$$

where $r_e \gg L$ is the distance from the fracture, where the far field pressure is determined, and r_0 is the radius of an equivalent vertical wellbore, having the same productivity as the fracture of length L.

Since the drawdown is uniform along the wellbore, $\Delta p_R(x) = \Delta p_{R0}$, the middle of the wellbore, can be chosen as a reference point for the calculation of the wellbore pressure

https://doi.org/10.1017/S0956792504005546 Published online by Cambridge University Press

p_F. Using (7.33) and assuming that $r_e \gg L$, we have

$$\Delta p_{R0} = \Delta p_R\left(\frac{L}{2}\right) = \frac{\mu q_0 \log r_e}{2\pi h k_H} - \frac{1}{\pi}\int_0^L \log\left|\frac{L}{2} - t\right| \psi(t)\,dt + \Pi_F \psi\left(\frac{L}{2}\right). \tag{9.4}$$

Using the evenness of the function $\psi(x)$ with respect to the middle of the wellbore, $x = L/2$, the following formula can be deduced:

$$\Delta p_{R0} = \frac{\mu q_0 \log r_e}{2\pi h k_H} + \Pi_F \psi\left(\frac{L}{2}\right) - \frac{2}{\pi}\int_0^{L/2} \log\left|\frac{L}{2} - t\right| \psi(t)\,dt, \tag{9.5}$$

which can be rewritten in dimensionless variables as

$$\Delta p_{R0} = \frac{\mu q_0}{2\pi h k_H}\left[\log\left(\frac{r_e}{L}\right) + \Omega\Psi\left(\frac{1}{2}\right) - 2\int_0^{1/2} \log\left(\frac{1}{2} - T\right)\Psi(T)\,dT\right]. \tag{9.6}$$

When $\Omega = 0$, one can use (6.5) to show that, the integral term in the RHS brackets is $2\log 2$, and therefore the drawdown Δp_{R0} matches the drawdown of a vertical fracture of infinite conductivity:

$$\Delta p_{R0} = \frac{\mu q_0}{2\pi h k_H} \log\left(\frac{4r_e}{L}\right). \tag{9.7}$$

Finally, the productivity ratio (8.2) is

$$\begin{gathered} I_0 = \log\left(\frac{4r_e}{L}\right)\left[\log\left(\frac{4r_e}{L}\right) + S_F(\Omega)\right]^{-1}, \\ \text{where} \quad S_F(\Omega) = \Omega\Psi\left(\frac{1}{2}\right) - 2\left[\log 2 + \int_0^{1/2} \log\left(\frac{1}{2} - T\right)\Psi(T)\,dT\right], \end{gathered} \tag{9.8}$$

where S_F can be considered as the additional skin, induced by the hydraulic resistance of the near wellbore zone. The advantage of the dimensionless parameter S_F compared to the productivity ratio is that it does not depend on the definition of the far field reservoir radius, r_e, and the far field pressure, p_e, but only on the parameter Ω, which characterises the reservoir and wellbore geometry (Fig. 12).

9.2 ICD calibration for uniform flux

Finally, let us consider a horizontal wellbore with uniform production profile. The reservoir pressure drawdown is shown in Fig. 13 (solid curve). The uniform pressure drawdown, which corresponds to the same production rate, is also shown for comparison (dashed line). As one could expect, the uniformity of the flux leads to nonuniform reservoir drainage, enhancing the risk of coning development in the middle part of the wellbore.

The hole density per ICD section, N_S, is shown in Fig. 14, for $N_{S0} = N_S(0) = 5, 6, 7$ and 8. An interesting result is that the solution of the inverse problem, $N_S(X)$, exists only for N_{S0} smaller than some critical number N^*_{S0}. In this case, $8 < N^*_{S0} < 9$. The attempt to

https://doi.org/10.1017/S0956792504005546 Published online by Cambridge University Press

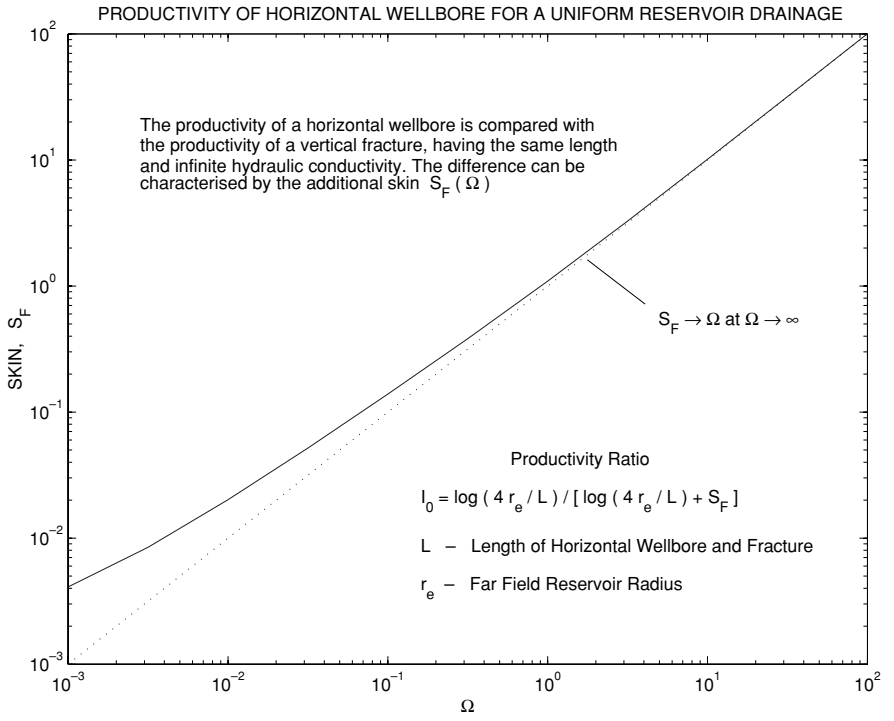

FIGURE 12. The skin, $S_F(\Omega)$, allows one to express the productivity of a horizontal wellbore through the productivity of the vertical fracture, having the same length.

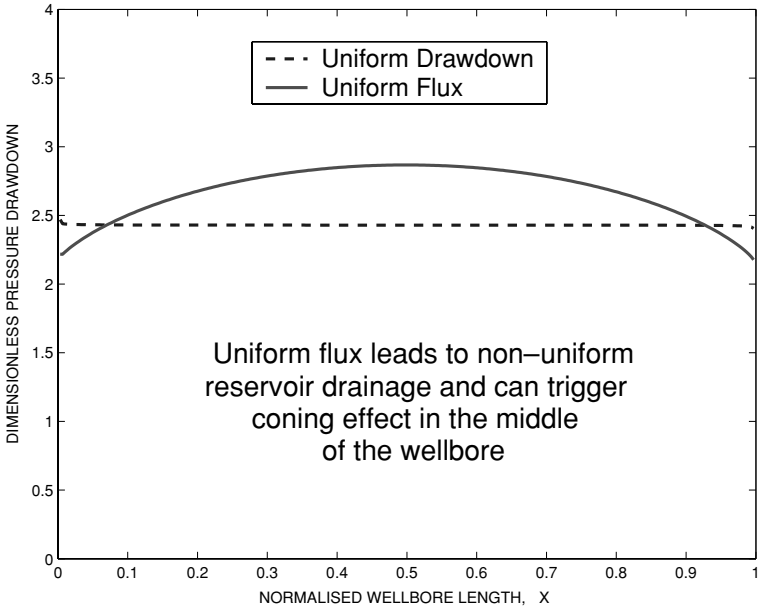

FIGURE 13. Reservoir pressure drawdown along the wellbore.

https://doi.org/10.1017/S0956792504005546 Published online by Cambridge University Press

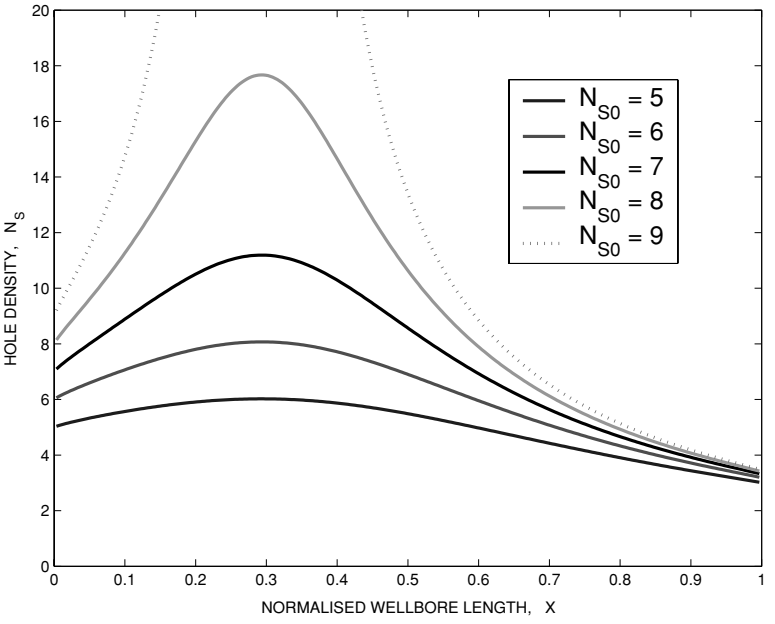

FIGURE 14. Hole density along the wellbore with uniform production profile.

calculate $N_S(X)$ for $N^*_{S0} = 9$, shown in Fig. 14 by the dashed curve, demonstrates that the hole density, N_S, becomes infinite somewhere in the middle of the wellbore. Inside the zone where $N_S = \infty$, the uniform flux cannot be achieved, and therefore this solution has to be rejected. The critical parameter N^*_{S0} is found from the requirement that $N_S(X) \to \infty$ at a single point in the middle of the wellbore. The solution of the inverse problem, which corresponds to this parameter N^*_{S0}, provides the ICD with uniform flux performance, having the highest hydraulic conductivity across it.

The explanation is that the uniform flux condition requires the suppression of fluxes near the end of the wellbore, which are exposed to larger drainage areas. This can be accomplished only by choosing relatively small hole densities near the wellbore ends. If the hole density is not small enough near the ends, the required pressure drawdown profile along the wellbore, shown in Fig. 13, cannot be achieved by an increase in the hole density in the middle part of the wellbore, where $N_S(X)$ obviously should have a maximum. At the same time, the smaller the parameter N_{S0} is, the flatter the hole density profile along the wellbore should be. Indeed, the higher the hydraulic resistance of the ICD is, the less is the difference between the two production regimes is, which correspond to *uniform drawdown* and *uniform flux*, as was demonstrated in Fig. 10 when $\Omega \to \infty$.

The drawdown across the ICD is shown in Fig. 15. One can see that the smaller the parameter N_{S0} is (i.e. the higher is the hydraulic resistance across the ICD), the more uniform is the drawdown across the ICD along the wellbore. At large N_{S0}, for example $N_{S0} = 8$, the flow restriction is needed mainly near the ends of the producing interval, whereas the drawdown across the ICD tends to zero in the middle part of the wellbore.

https://doi.org/10.1017/S0956792504005546 Published online by Cambridge University Press

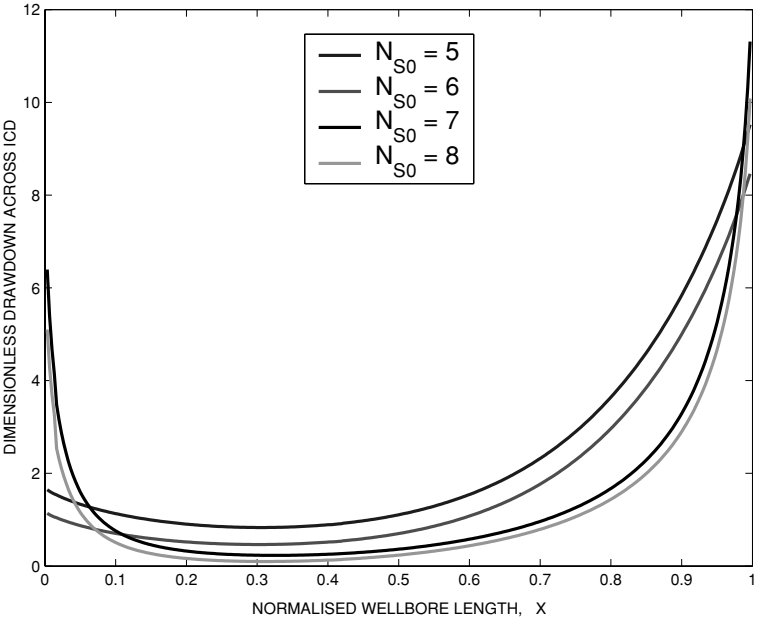

FIGURE 15. Drawdown across the ICD along the wellbore with uniform production profile.

10 Conclusions

- A model of steady single-phase flow into a horizontal wellbore with Inflow Control Device (ICD) in an anisotropic reservoir has been developed. This model is based on the concept of flow structuring, and it allows one to reduce a complicated three-dimensional problem to a one-dimensional singular integro-differential equation, which can be efficiently solved numerically.
- The flow pattern around a horizontal wellbore has been investigated. We have represented it by the flow around a vertical fracture, having the same length with an additional skin distributed along its length.
- The inverse problem of calibration of the ICD has been formulated and solved, allowing one to find the open area of the basepipe that is required to achieve either uniform drawdown or a desired influx distribution along the horizontal wellbore.
- We have demonstrated that the optimal hole density of the basepipe is not affected very much by changes in the production rate, and therefore the ICD can be effectively tuned just once before installation to provide a required flow control during the entire production life of the wellbore.
- An extension of the model should allow one to investigate the transient cleanup of a horizontal wellbore, surrounded by an invasion zone with impaired hydraulic conductivity, during the initial phase of production.

https://doi.org/10.1017/S0956792504005546 Published online by Cambridge University Press

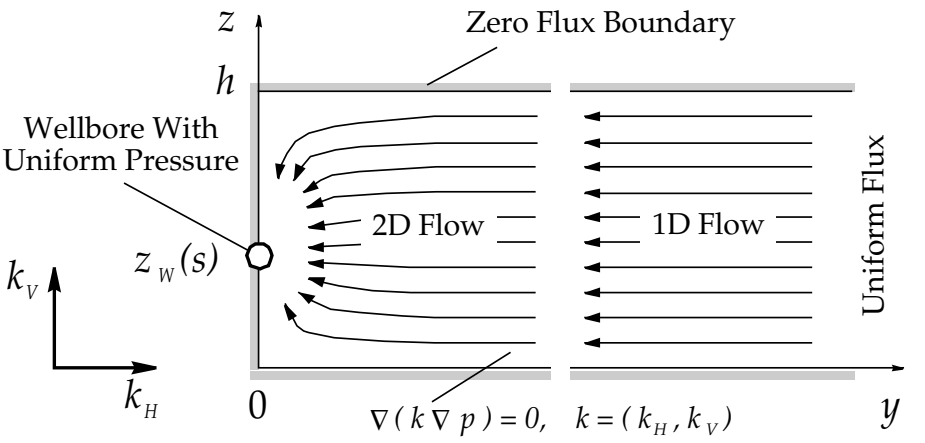

FIGURE A.1. The local 2D flow near the horizontal wellbore.

Appendix A Local two-dimensional flow near a horizontal wellbore

The geometry of the problem to be investigated is shown in Fig. A.1.

We are looking for the solution of the modified Laplace equation

$$\frac{\partial^2 p}{\partial y^2} + \frac{1}{\omega^2}\frac{\partial^2 p}{\partial z^2} = 0, \quad \omega = \sqrt{\frac{k_H}{k_V}} \tag{A.1}$$

which satisfies zero-flux conditions at its horizontal boundaries,

$$\left.\frac{\partial p}{\partial z}\right|_{z=0} = \left.\frac{\partial p}{\partial z}\right|_{z=h} = 0, \tag{A.2}$$

and has uniform pressure distribution along the wellbore surface

$$p = \text{const.}, \quad y^2 + (z - z_W)^2 = r_W^2. \tag{A.3}$$

This solution also has to match the flux into the equivalent vertical fracture at a large distance from the wellbore, where the flow is horizontal:

$$\left.\frac{\partial p}{\partial y}\right|_{y\to\infty} = \psi(x). \tag{A.4}$$

A.1 Outer solution

The solution of the problem (A.1)–(A.4) at large distance from the wellbore should not be sensitive to the local flow pattern near the wellbore. It should only depend upon the local production rate across the unit wellbore length:

$$q_W(x) = \frac{2hk_H}{\mu}\psi(x), \tag{A.5}$$

https://doi.org/10.1017/S0956792504005546 Published online by Cambridge University Press

and we assume that the ratio of the wellbore radius to the reservoir thickness is small:

$$\varepsilon = r_W/h \ll 1. \tag{A.6}$$

This means that one can neglect the boundary condition on the wellbore (A.3), and replace the wellbore by a point source with the appropriate strength. The solution of this problem can be found using the method of images [9]. If we introduce the outer coordinates $\bar{y} = \frac{y}{h}$ and $\bar{z} = \frac{z}{h}$, the result is

$$p_1 = p_0(x)P_1(\bar{y},\bar{z}), \quad p_0(x) = \frac{\omega h}{2\pi}\psi(x) \tag{A.7}$$

$$P_1(\bar{y},\bar{z}) = \log\left\{\cosh\left(\frac{\pi\bar{y}}{\omega h}\right) + \cos\left[\frac{\pi}{h}(\bar{z}+\bar{z}_W-h)\right]\right\} + \log\left\{\cosh\left(\frac{\pi\bar{y}}{\omega h}\right) - \cos\left[\frac{\pi}{h}(\bar{z}-\bar{z}_W)\right]\right\}. \tag{A.8}$$

We call $p_1(\bar{y},\bar{z})$ the outer solution of the problem (A.1)–(A.4). This solution involves also an additive arbitrary constant, which has been chosen above equal to zero. One can verify that the dimensionless pressure $P_1(\bar{y},\bar{z})$, given by (A.8), has a logarithmic singularity in the middle of the wellbore, where the source point is located.

The solution (A.7) could be used for the approximate determination of the wellbore pressure by averaging $P_1(\bar{y},\bar{z})$ over the wellbore surface $\bar{y}^2 + (\bar{z}-\bar{z}_W)^2 = \varepsilon^2$.

When the reservoir permeability is isotropic, i.e. $\omega = 1$, then the outer solution (A.7) satisfies the condition (A.3) with the error $o(\varepsilon)$. In this case, the dimensionless wellbore pressure is

$$P_{1W} \approx \log\left\{1 + \cos\left[\pi\left(\frac{2\bar{z}_W}{h} - 1\right)\right]\right\} + 2\log\left(\frac{\pi\varepsilon}{\sqrt{2}}\right). \tag{A.9}$$

Unfortunately, if $\omega \neq 1$, the outer solution (A.6) generates at the wellbore a nonuniform pressure, and therefore the requirement (A.3) is not satisfied even approximately. This means that the outer solution does not match the local pressure behaviour at the wellbore, and has to be corrected. One can achieve this, considering the asymptotic solution of the problem (A.1)–(A.4) near the wellbore, which we subsequently call the inner solution.

A.2 Inner solution

Let us introduce the inner coordinates with the origin in the centre of the wellbore:

$$\bar{y} = \varepsilon Y, \quad \bar{z} - \bar{z}_W = \frac{\varepsilon Z}{\omega}. \tag{A.10}$$

The geometry of the problem in these coordinates is shown in Fig. A2.

The modified Laplace equation (A.1) becomes the conventional Laplace equation in these coordinates:

$$\frac{\partial^2 p}{\partial Y^2} + \frac{\partial^2 p}{\partial Z^2} = 0. \tag{A.11}$$

https://doi.org/10.1017/S0956792504005546 Published online by Cambridge University Press

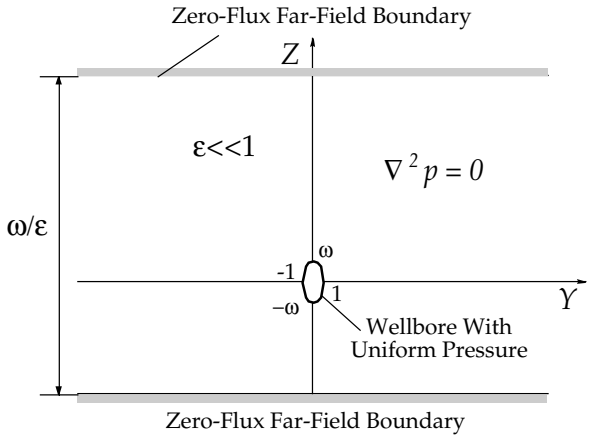

FIGURE A.2. The flow into the elliptic wellbore inside the thick isotropic layer.

At the same time, the circular wellbore wall becomes an ellipse

$$Y^2 + \left(\frac{Z}{\omega}\right)^2 = 1. \tag{A.12}$$

The local solution of the Laplace equation (A.11) around the elliptic hole with uniform pressure at its boundary (A.12) can be easily found if one neglects all other boundary conditions, which become the far field conditions in the inner coordinates (A.10). The wellbore radius is indeed of the order of 1 in these coordinates whereas the distance to the reservoir boundaries is of the order of $\varepsilon^{-1} \gg 1$.

Let us consider the elliptic coordinate system with the origin in the centre of the wellbore:

$$Y = c \sinh \xi \sin \eta, \quad Z = c \cosh \xi \cos \eta \tag{A.13}$$

Here ξ is similar to the radial distance, η is the angle and c is an arbitrary constant, which has to be chosen from a set of additional conditions.

The advantage of the elliptic coordinates, ξ and η, over the Cartesian ones, Y and Z, is two-fold: (1) the transformation $(Y, Z) \rightarrow (\xi, \eta)$ fulfils the conformal mapping, which preserves angles between curves on the planes (Y, Z) and (ξ, η); and (2) the confocal ellipses on the plane (Y, Z) have very simple equations in the plane (ξ, η): $\xi = \text{const}$. Indeed, eliminating η between (A.13), one has

$$\left(\frac{Y}{c \sinh \xi}\right)^2 + \left(\frac{Z}{c \cosh \xi}\right)^2 = 1. \tag{A.14}$$

To match the ellipse (A.12), which corresponds to the wellbore, at $\xi = \xi_0 = \text{const.}$, one has to choose the parameters c and ξ_0 from the conditions

$$c \sinh \xi_0 = 1, \quad c \cosh \xi_0 = \omega, \tag{A.15}$$

https://doi.org/10.1017/S0956792504005546 Published online by Cambridge University Press

resulting in

$$c = \sqrt{\omega^2 - 1}, \quad \xi_0 = \log \sqrt{\frac{\omega + 1}{\omega - 1}}. \tag{A.16}$$

This solution is valid for $\omega > 1$ only, which is usually the case. If, however, $\omega < 1$, then one has to introduce the coordinates (ξ, η) as follows:

$$Y = c \cosh \xi \cos \eta, \quad Z = c \sinh \xi \sin \eta, \tag{A.17}$$

instead of (A.13). We shall assume, however, for the time being that $\omega > 1$.

The solution of the Laplace equation (A.11), which satisfies the condition $p = \text{const}$ at the wellbore surface $\xi = \xi_0$, is

$$p_2 = p_0(x) P_2(Y, Z), \quad P_2(Y, Z) = C_1 + C_2 \xi, \tag{A.18}$$

where C_1 and C_2 are the parameters to be determined, $p_0(x)$ is the same as in (A.6), and P_2 is the dimensionless pressure.

A.3 Asymptotic matching

The parameters C_1 and C_2 have to be chosen from the condition that the inner and outer solutions overlap somewhere in the middle zone, which is far from the wellbore, and also far from the external boundaries – the top and bottom of the reservoir in our case. This can be achieved, using the method of matched asymptotic expansions [16].

To construct the global solution of the problem (A.1)–(A.4), we require that the far field behaviour of the inner solution P_2 in the stretched coordinates Y, Z matches the local behaviour of the outer solution P_1 in the same coordinates, i.e.

$$\lim_{\xi \to \infty} P_2(Y, Z) = \lim_{\xi \to 0} P_1 \left(\varepsilon h Y, \frac{\varepsilon h Z}{\omega} + z_W \right). \tag{A.19}$$

Using (A.7) and (A.8), one obtains the leading terms of the asymptotic behaviour of the outer solution P_1 for small Y and Z

$$P_1 \approx \log \left\{ 1 + \cos \left[\pi \left(\frac{2 z_W - h}{h} \right) \right] \right\} + 2 \log \left(\frac{\pi \varepsilon}{\omega} \right) - \log 2 + \log(Y^2 + Z^2). \tag{A.20}$$

Using the expansion

$$\log(Y^2 + Z^2) = 2 \log \left(\frac{c}{2} \right) + 2\xi - 2 \sum_{n=1}^{\infty} \frac{(-1)^n}{n} e^{-2n\xi} \cos(2n\eta), \tag{A.21}$$

one can write

$$\lim_{\xi \to \infty} P_2(Y, Z) = \frac{C_2}{2} \log(Y^2 + Z^2) - C_2 \log \left(\frac{c}{2} \right) + C_1, \tag{A.22}$$

and therefore the unknown parameters C_1 and C_2 have to be chosen as

$$C_1 = \log \left\{ 1 + \cos \left[\pi \left(\frac{2 z_W - h}{h} \right) \right] \right\} + 2 \log \left(\frac{\pi \varepsilon}{\omega} \right) - \log 2 + 2 \log \left(\frac{c}{2} \right), \quad C_2 = 2. \tag{A.23}$$

https://doi.org/10.1017/S0956792504005546 Published online by Cambridge University Press

This allows one to obtain the dimensionless pressure at the wellbore, P_{1W}, which corresponds to $\xi = \xi_0$. Using (A.18), (A.23) and (A.16), we arrive at the following expression:

$$P_{1W} = C_1 + C_2\xi_0 = \log\left\{1 + \cos\left[\pi\left(\frac{2z_W - h}{h}\right)\right]\right\} + 2\log\left(\frac{\pi\varepsilon}{\omega}\right) - \log 2 + \log\left(\frac{\omega^2 - 1}{4}\right) + \log\left(\frac{\omega + 1}{\omega - 1}\right) = \log\left\{1 + \cos\left[\pi\left(\frac{2z_W - h}{h}\right)\right]\right\} + 2\log\left[\frac{\pi\varepsilon(\omega + 1)}{2\sqrt{2}\omega}\right]. \quad \text{(A.24)}$$

This result is valid not only for $\omega > 1$, but also for an arbitrary permeability anisotropy ratio ω ($0 < \omega < \infty$), and it matches the solution (A.9), which has been obtained above for $\omega = 1$.

Appendix B ICD calibration for uniform reservoir drainage

We consider below a few series of calculations, which have been carried out for the data, corresponding to a conceptual reservoir model with characteristics similar to certain North Sea provinces [2]:

Production rate	$q_0 = 33$ & $66\,\mathrm{m}^3/h = 5$ & $10\,kbbl/\mathrm{day}$
Wellbore length	$L = 1200\,\mathrm{m}$
Reservoir thickness	$h = 24\,\mathrm{m}$
Horizontal permeability	$k_H = 700\,\mathrm{mD}$
Vertical permeability	$k_V = 350\,\mathrm{mD}$
Wellbore radius	$r_W = 0.0762\,\mathrm{m}$
Internal radius of ICD basepipe	$r_S = 0.038\,\mathrm{m}$
Diameter of holes in basepipe	$d_P = 0.003\,\mathrm{m}$
Fluid viscosity	$\mu = 1\,\mathrm{cp}$
Fluid density	$\rho = 750\,\mathrm{kg/m}^3$
Length of ICD section	$L_S = 3.66\,\mathrm{m} = 12\,\mathrm{ft}$

We assumed that the horizontal wellbore is parallel to the reservoir boundaries, and it is located in middle of the reservoir thickness. The far field reservoir pressure has been determined at the distance $r_e = L/2$ from the wellbore along the plane perpendicular to its trajectory. The parameter Ω was therefore constant along the wellbore and equal to 0.135.

We started from the determination of the optimal hole densities (per ICD section) needed to achieve a uniform reservoir drainage for two production rates (5 kB/D and 10 kB/D), $N_S^{(5)}(X)$ and $N_S^{(10)}(X)$. The solutions of the forward problem (i.e. the flux and the pressure drawdown), corresponding to both hole densities, have then been found for each production rate and compared. This allowed us to estimate the effect of deviation from the production regime on the reservoir drainage for a passive flow control device, which can be tuned only once before installation.

https://doi.org/10.1017/S0956792504005546 Published online by Cambridge University Press

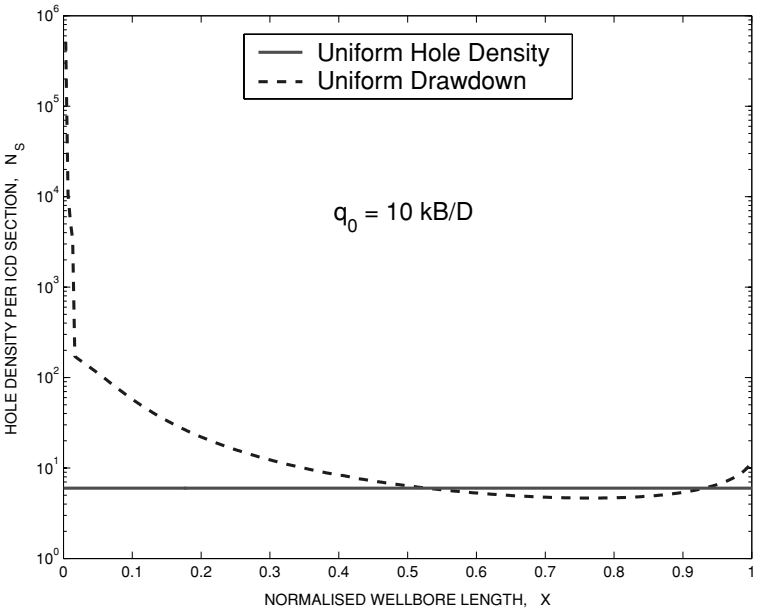

FIGURE B.1. Hole density along the wellbore length.

Case I

The production rate, q_0, was equal to 10 kB/D. First, the inverse problem has been solved and the optimal hole density, $N_S(X)$, has been determined. This hole density then was used to solve the forward problem. The obtained flux and pressure along the wellbore have been compared with the solution, corresponding to the uniform hole density, $N_S(X) = N_{S0}$, which has been found by averaging the entire hydraulic resistance of the ICD, i.e.

$$N_{S0}^{-2} = \int_0^1 N_S^{-2}(X)\, dX \tag{B.1}$$

The optimal hole density is shown in Fig. B.1 by a dashed curve. The uniform hole density N_{S0} occurred to be equal to 7 in this case. One can clearly see the steep drop in the optimal hole density near the toe, which is explained by the transition of the laminar flow in the basepipe to the turbulent one. Thus, except the short initial interval near the toe, the flows is turbulent in the basepipe. This transition is accompanied by an increase in frictional pressure losses along the wellbore and, for this reason, further restriction of the hydraulic conductivity of the ICD downstream is required.

The slight increase in the hole density near the heel can be explained by the flux behaviour near the ends of the producing interval of the horizontal wellbore, shown in Fig. B.2, which is much more pronounced for the optimal hole density. The uniform reservoir drawdown generates a symmetrical flux distribution with respect to the middle of the wellbore (dashed curve) whereas the flux, corresponding to the uniform hole density, is asymmetrical (solid curve) with a substantial increase near the heel. For the uniform hole density, the horizontal wellbore under-produces near the toe and the heel but over-produces in the middle part of the wellbore.

https://doi.org/10.1017/S0956792504005546 Published online by Cambridge University Press

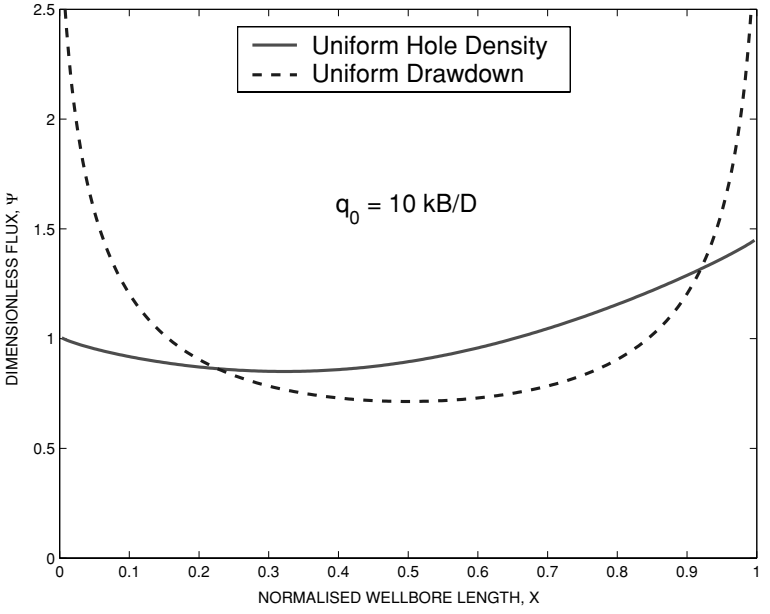

FIGURE B.2. Flux along the horizontal wellbore.

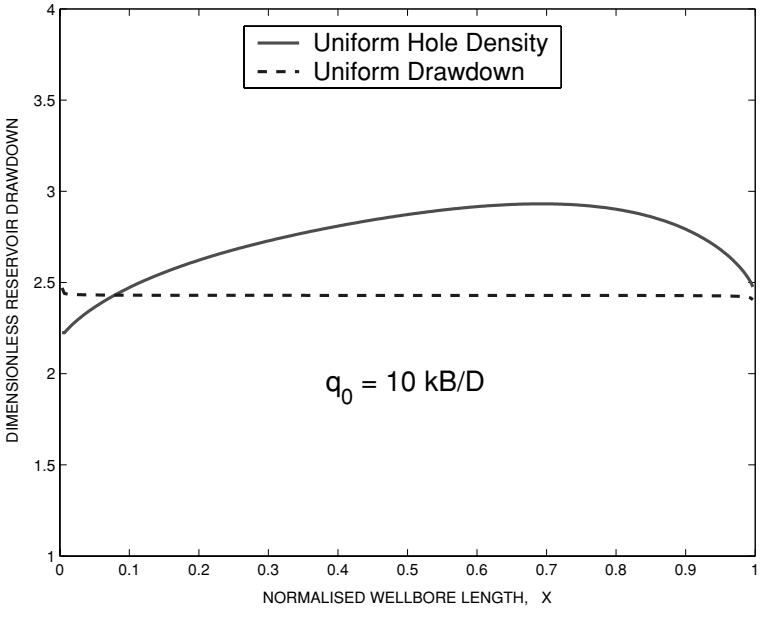

FIGURE B.3. Reservoir pressure drawdown along the wellbore.

This results in the reservoir drawdown behaviour, shown in Fig. B.3. For the uniform hole density, the drawdown has a maximum at approximately one third of the wellbore length from its heel. If such an ICD is installed, coning near the heel of the horizontal wellbore may occur.

https://doi.org/10.1017/S0956792504005546 Published online by Cambridge University Press

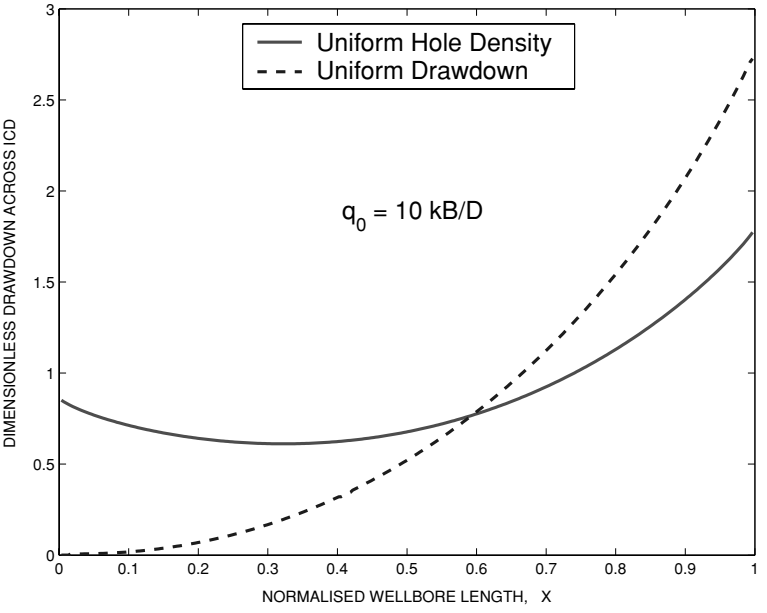

FIGURE B.4. Drawdown across the ICD along the wellbore.

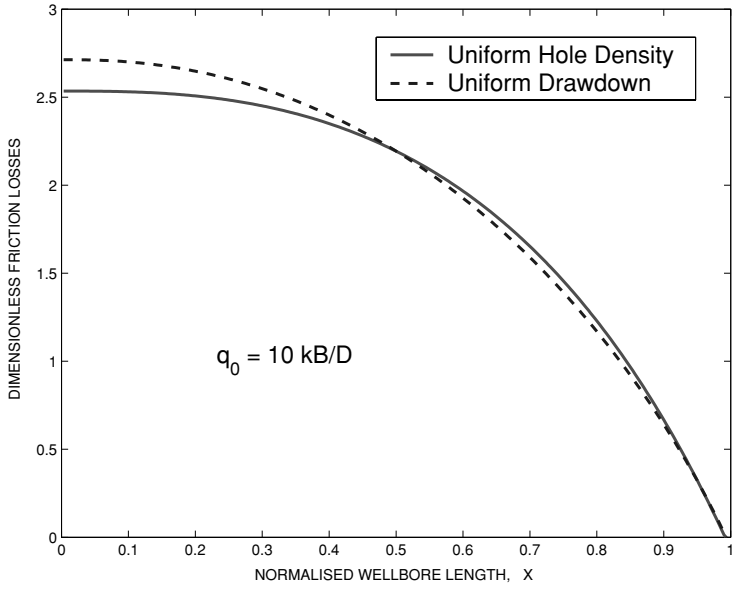

FIGURE B.5. Wellbore pressure profile inside the ICD basepipe.

The drawdown across the ICD and the frictional pressure losses along then wellbore are shown in Figs. B.4 and B.5, respectively. At the optimal hole density, the drawdown across the ICD compensates completely for the frictional pressure losses along the wellbore. The drawdown across the ICD for the uniform hole density is flatter and therefore the frictional pressure drop along the wellbore is not fully compensated.

https://doi.org/10.1017/S0956792504005546 Published online by Cambridge University Press

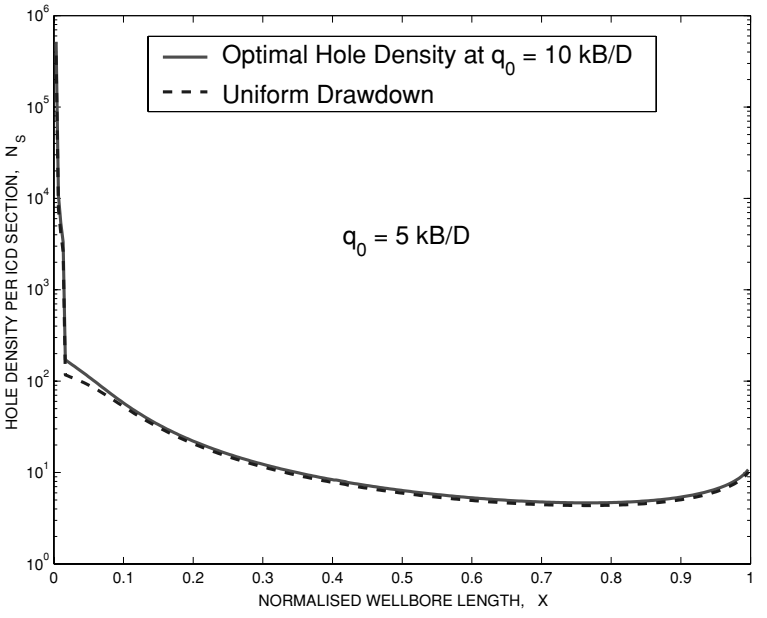

FIGURE B.6. Hole density along the wellbore length at two production rates.

The wellbore pressure profiles along the ICD basepipe, which are shown in Fig. B.5, are normalised with respect to the pressures at the heel ($X = 1$). One can see that, although the difference between the total pressure drops along the wellbore due to friction is of the order of 10% in the two cases, the maximum reservoir drawdown, shown in Fig. B.6, is of the order of 50% of the minimal drawdown at the toe of the wellbore. This is the typical situation where the frictional pressure losses inside the basepipe are comparable with the applied reservoir drawdown.

Case II

In this series of calculations, the production rate, q_0, was halved and the forward problem was then solved for two profiles of hole densities: the optimal one, corresponding to the current production rate $q_0 = 5\,\mathrm{kB/D}$; and the hole density, found above for $q_0 = 10\,\mathrm{kB/D}$. The results are shown in Figs. B.6–B.10.

The differences between the two computed hole densities are really small (see Fig. B.6), as well as the differences between the fluxes (Fig. B.7) and the reservoir drawdowns (Fig. B.8), everywhere except the heel neighbourhood. These results are consistent with the correlation (7.19). The differences between the pressure drops across the ICD are substantial near the heel of the wellbore due to differences in flux in this zone (Fig. B.9), but are very small along the rest of the wellbore. The frictional pressure losses are smaller than at doubled production rate ($q_0 = 10\,\mathrm{kB/D}$) but again are rather close to each others (Fig. B.10).

These results confirm the expectation, based on the relationship (7.19), that the initial calibration of the ICD should allow one to maintain a uniform or close to uniform pressure drawdown for a wide range of production rate.

https://doi.org/10.1017/S0956792504005546 Published online by Cambridge University Press

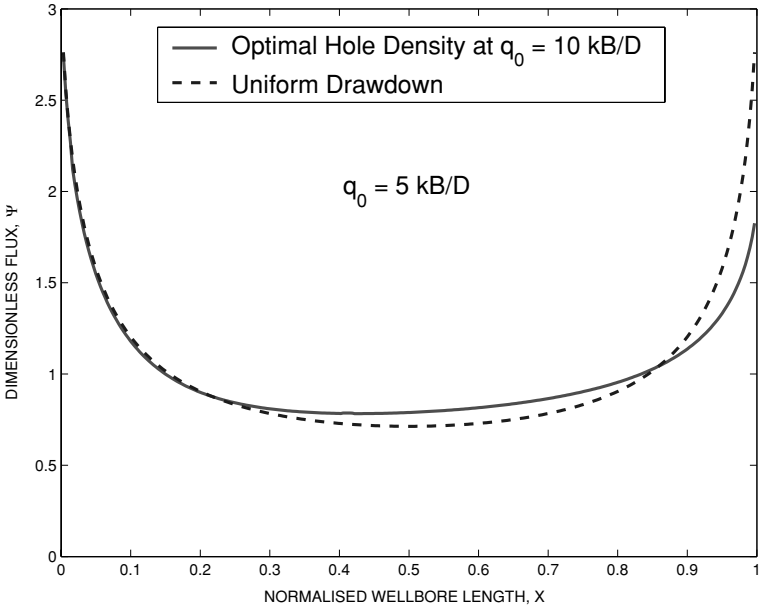

FIGURE B.7. Flux along the horizontal wellbore.

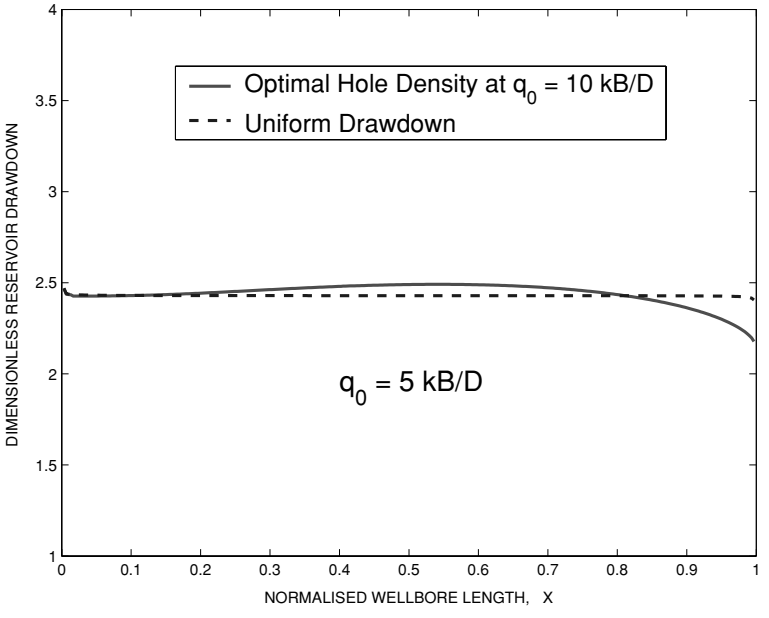

FIGURE B.8. Reservoir drawdown along the wellbore.

Case III

In this series, the same calculations were carried out for the production rate $q_0 = 10\,\mathrm{kB/D}$. The optimal hole density profiles calculated for $q_0 = 5\,\mathrm{kB/D}$ and $q_0 = 10\,\mathrm{kB/D}$, which are shown in Fig. B.6, were used. The results are presented in Figs. B.11–B.14.

https://doi.org/10.1017/S0956792504005546 Published online by Cambridge University Press

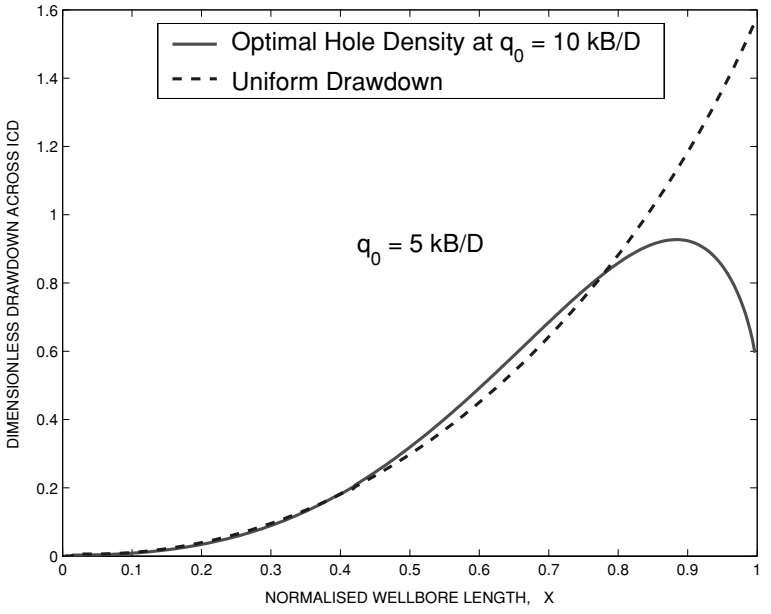

FIGURE B.9. Drawdown across the ICD along the wellbore.

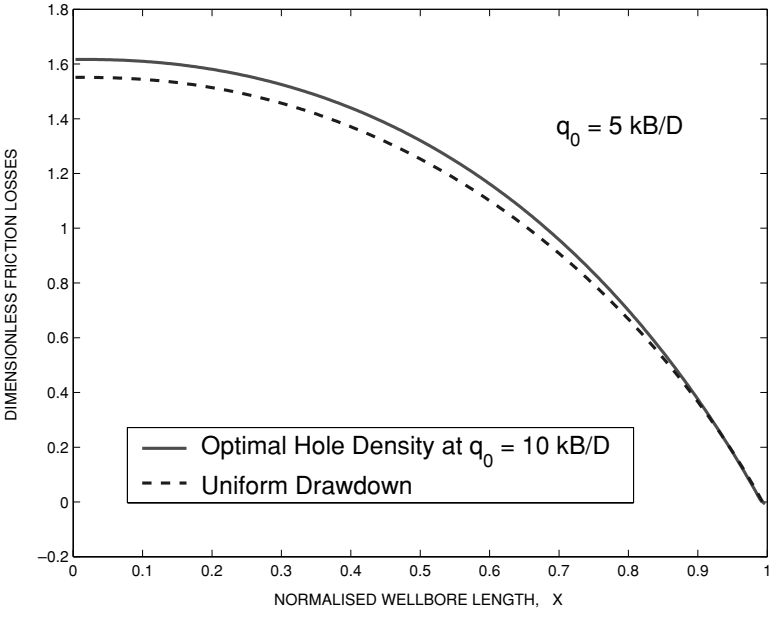

FIGURE B.10. Wellbore pressure profile inside the ICD basepipe.

One can see that the increase in production rate affects the flux along the wellbore in the same way the decrease in production rate did (Fig. B.11). The flux goes up with respect to the optimal flux in the middle part of the wellbore and down near the heel. The reservoir drawdown changes modestly (Fig. B.12). The changes in the pressure drop across

https://doi.org/10.1017/S0956792504005546 Published online by Cambridge University Press

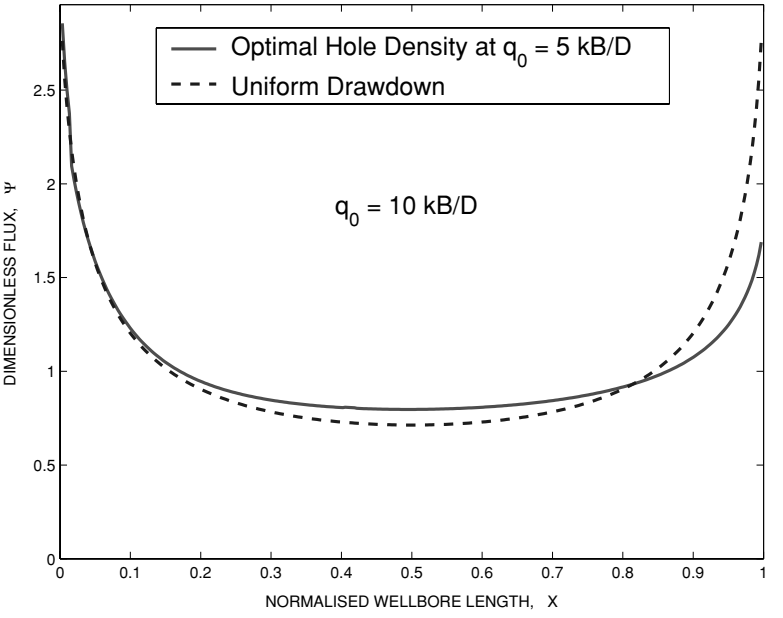

FIGURE B.11. Flux along the horizontal wellbore.

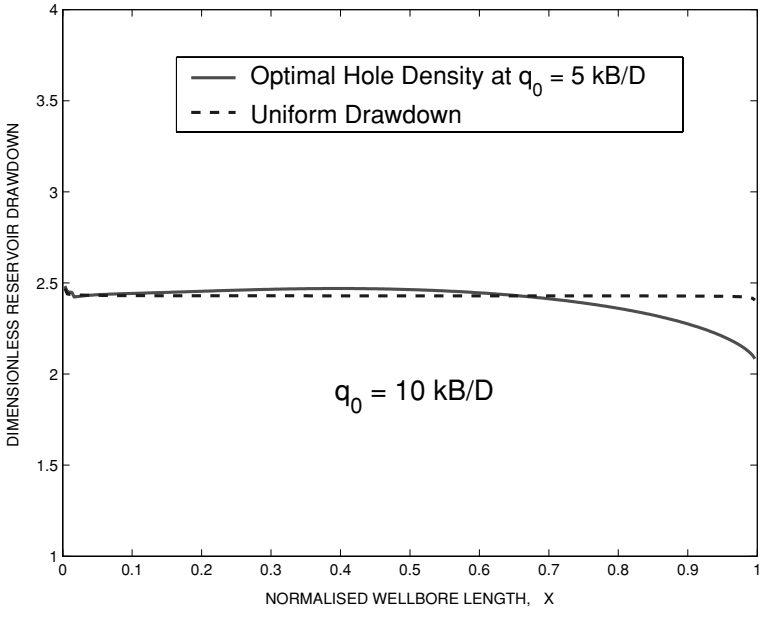

FIGURE B.12. Reservoir drawdown along the wellbore.

the ICD are more pronounced than in the case of smaller production rate $q_0 = 5\,\mathrm{kB/D}$ (Fig. B.13). The frictional pressure losses are higher at higher production rate and the change with the increased production rate is also more pronounced (Fig. B.14).

https://doi.org/10.1017/S0956792504005546 Published online by Cambridge University Press

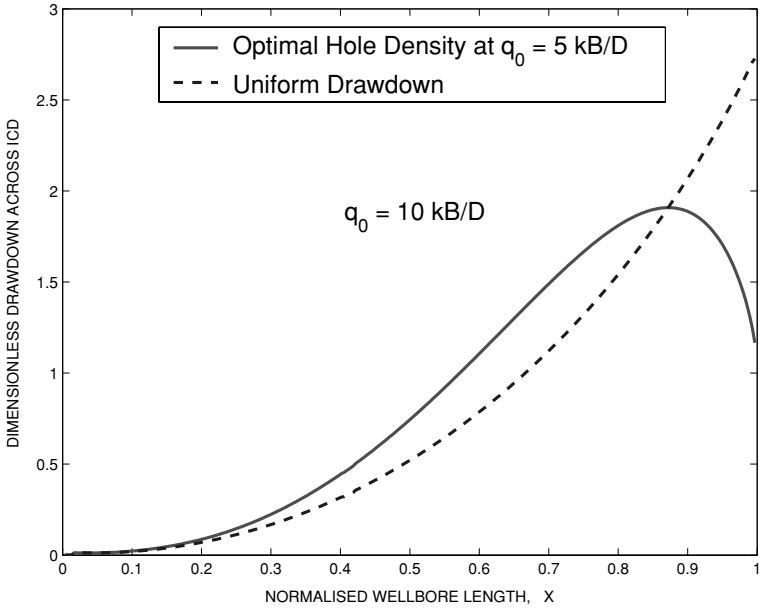

FIGURE B.13. Drawdown across the ICD along the wellbore.

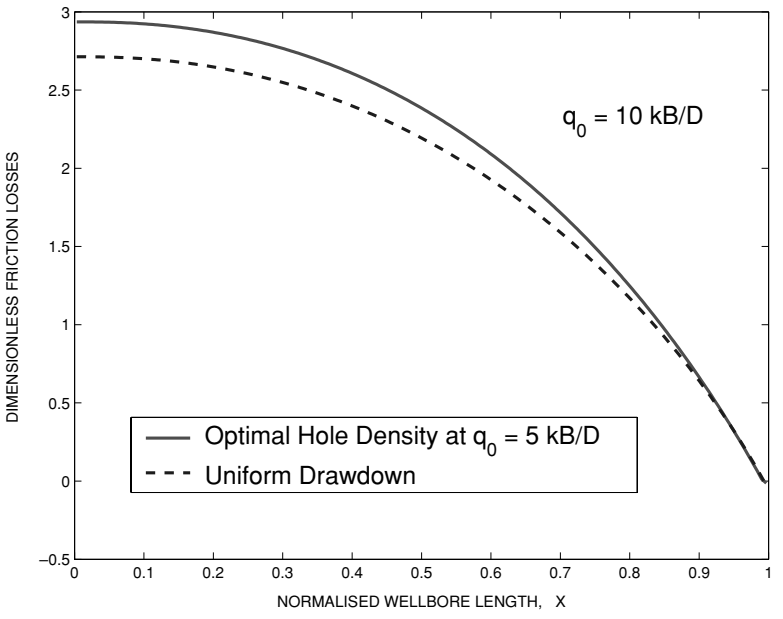

FIGURE B.14. Wellbore pressure profile inside the ICD basepipe.

The examples considered above clearly demonstrate the importance of calibration of the ICD to achieve a uniform reservoir drainage, and therefore to prevent the manifestation of the coning effect. The good news is that the ICD tuning, which is supposed to be done only once, just before the installation, should guarantee a good performance within a wide range

https://doi.org/10.1017/S0956792504005546 Published online by Cambridge University Press

of variation of the production rate. One should thus expect that the installation of an ICD, which is a passive flow control device, can be considered as a valuable complementary option to the package of services available now for the horizontal well completions.

Acknowledgements

The authors would like to convey their acknowledgement to Craig Johnson and Xavier Lopez, who started this project and provided a lot of support, and also to Pat Bixenman and Younes Jalali for the multiple discussions, constructive suggestions and general encouragement.

References

[1] Bateman, H. (1964) *Partial Differential Equations of Mathematical Physics*. Cambridge University Press.
[2] Betancourt, S., Dahlberg, K., & Jalali, Y. (2002) Natural Gas-Lift: Theory and Practice. SPE 74391.
[3] Brekke, K., Johansen, T. E. & Olufsen, R. (1993) A new modular approach to comprehensive simulation of horizontal wells. SPE Paper 26518.
[4] Chaperon, I. (1986) Theoretical study of coning toward horizontal and vertical wells in anisotropic formations: subcritical and critical rates. SPE Paper 15377.
[5] Dikken, B. J. (1990) Pressure drop in horizontal wells and its effect on production performance. SPE Paper 19824.
[6] Folefac, A. N., Archer, J. S., Issa, R. I. & Arshad, A. M. (1991) Effect of pressure drop along horizontal wellbores on well performance. SPE Paper 23094.
[7] Joshi, S. D. (1991) *Horizontal Well Technology*. PennWell Publishing Co., Tulsa, OK.
[8] Kuchuk, F. J., Lenn, C., Hook, P. & Fjerstad, P. (1998) Performance evaluation of horizontal wells. SPE Paper 39749.
[9] Landman, M. J. & Goldthorpe W. H. (1991) Optimization of perforation distribution for horizontal wells. SPE Paper 23005.
[10] Lifanov, I. K. (1996) *Singular Integral Equations & Discrete Vortices*. VSP Utrecht.
[11] Loitsyanskii, L. G. (1966) *Mechanics of Liquids and Gases*. Pergamon, Oxford.
[12] Marret, B. P. & Landman, M. J. (1993) Optimal perforation design for horizontal wells with boundaries. SPE Paper 25366.
[13] Miller, D. S. (1990) *Internal Flow Systems, 2nd Ed*. BHRA, p. 345.
[14] Prats, M. (1961) Effect of vertical fracture on reservoir behavior – incompressible fluid case. *SPE J.* **1**, 105–118.
[15] Tang, Y., Ozkan, E., Kelkar, M., Sarica, C. & Yildiz, T. (2000). Performance of horizontal wells completed with slotted liners and perforations. SPE Paper 65516.
[16] Van Dyke, M. D. (1975) *Perturbation Methods in Fluid Mechanics*. The Parabolic Press, Stanford, CA.
[17] Yuan, H., Sarica, C. & Brill, J. P. (1998) Effect of completion geometry and phasing on single-phase liquid flow behavior in horizontal wells. SPE Paper 48937.
[18] Zazovsky, A. F. (1994) A pseudoskin factor for a partially penetrating hydraulic fracture. SCR Report SCR/SR/1994/036/IGM/C.